ENGINEERING RESEARCH INSTITUTE
UNIVERSITY OF MICHIGAN
ANN ARBOR

FINAL REPORT

WING-BODY INTERFERENCE

PART III. EXPERIMENTAL INVESTIGATION OF BODY SIMULATOR PLATE

By

H. E. BAILEY

R. E. PHINNEY

Projects M937 and M937-1

WRIGHT AIR DEVELOPMENT CENTER, U.S. AIR FORCE
CONTRACT AF 33(038)-19747, E.O. NO. 460-31-12-11 SR-1g

February, 1954

TABLE OF CONTENTS

LIST OF FIGURES

FINAL REPORT

WING-BODY INTERFERENCE

PART III. EXPERIMENTAL INVESTIGATION OF BODY SIMULATOR PLATE

A. INTRODUCTION

This is the third and last section of the final report on Contract AF 33(038)19747 and presents the experimental results obtained from the wing-body simulator model which is described in section C. Before proceeding to a description of the model and a detailed discussion of the test results obtained, it is perhaps wise to discuss in general terms the configurations tested.

B. NONREFLECTING OR GRAZING TYPE OF SHOCK-WAVE - BOUNDARY-LAYER INTERACTION

When a shock wave impinges on a flat surface the shock wave tends to deflect the flow into the surface so that a reflected wave deflecting the flow in the opposite direction is needed to make the resulting flow follow the surface. Thus the boundary brings about an approximate doubling of the pressure rise associated with the original impinging shock wave if the line of impingment is normal to the free-stream velocity. This increased pressure rise will in turn increase the boundary-layer disturbance.

On the other hand, when a two-dimensional wing terminates in a vertical end plate the shock wave from the wing will cause flow deflections only in the plane of the plate, so that no reflected wave is generated. The boundary layer on the end plate is therefore subjected to only the single pressure rise due to the original shock wave. Furthermore the pressure gradient in this case

will have a component perpendicular to the flow direction upstream of the shock. Henceforth, this type of shock - boundary-layer interaction will be referred to as a nonreflecting or grazing-shock - boundary-layer interaction. Several examples of this grazing type of interaction which occur frequently are the juncture between a wing and the wind tunnel wall in two-dimensional testing, the interactions present on cruciform tails, the juncture region of wing and body, etc.

Some feeling for the three-dimensional flow in the boundary layer on the end plate might be obtained by treating the idealized case of the swept-back nonreflecting shock wave extended to infinity, similar to the manner in which the boundary layer on swept wings is treated in subsonic flow. This approach cannot of course account for the transient region near the juncture of the two plates, nor can it take into account the fact that the Reynolds' number of the boundary layer on the flat plate will vary along the shock wave. This local sweepback approach is of course further limited in that it is strictly applicable only for a laminar boundary layer.

The qualitative experience accumulated in the present experiments from the china-film patterns of the inner boundary-layer flow shows that at least two distinct patterns of behavior of the boundary-layer flow on the plate occur in the presence of a grazing shock wave.

If the shock wave is weak, the china-clay patterns indicate a narrow, slowly widening dark band which is a region of decreased shear in the boundary layer at the front of the shock and a slight deflection of the inner part of the boundary layer. This widening of the region of decreased shear in the boundary layer is probably associated to some extent with the increasing thickness of the boundary layer along the trace of the shock. The local deflection angle indicated by the pattern is likely to exceed the corresponding deflection across the grazing shock wave outside the boundary layer, since the low-inertia inner layer is more responsive to the same lateral pressure gradient.

When the grazing shock wave is strong, the dark band is much wider and is followed by an angular sector where the inner layer appears to flow radially along the trace of the shock wave. The transition from the radial flow to the after flow, where the inner layer presumably tends to follow the outer streamlines, again is not clear. Sometimes it appears gradually, while sometimes there appears to be a sharp line indicating the downstream limit of the radial-flow region.

From existing experience obtained in the case of reflected shock-wave - boundary-layer interaction and qualitative application of the viscous sweepback principle, it may be conjectured that the boundary layer on the plate must separate locally under the influence of a sufficiently strong pressure gradient. The separated air would then probably tend to flow in the

general direction of the shock trace. At its foot the grazing shock may then spread into continuous gradients or it may even bifurcate; thus there may be a central expansion wave over the top of the separated flow. No pressure distributions are available under or near the foot of the grazing shock for the case of very strong waves, but it is possible that a double-bump pressure distribution similar to those reported in reference 1 may exist.

If the experience previously obtained in the case of shock-wave reflections from laminar boundary layers is applied to the grazing type of interaction, it may be conjectured that the laminar boundary layer will separate for considerably weaker shock waves than does the turbulent boundary layer. Furthermore, the separation itself may be expected to be more extensive.

Patterns of the second type, i.e., those associated with a strong grazing shock wave were observed with the turbulent boundary layer only for extremely strong shock waves, i.e., flow deflection angles of the order of 20°. However, if the boundary layer is laminar it is possible to obtain somewhat similar effects for small flow deflections of the order of 8°.

Near the leading edge, as the wing pierces the boundary layer on the plate, the picture of the simple grazing interaction just presented may be modified. Outside the plate boundary layer the shock wave may be considered attached to the wing, at least on the compression side of the wing. On the expansion side of the wing, however, it has been observed[1,2] that a very weak shock wave precedes the expansion wave. This is attributed to the finite thickness of the leading edge of the wing, which causes a local detachment of the shock wave at the leading edge. The weak compression shock is then the continuation of the shock wave which occurs on the compression side of the wing. When the deflection angle on the compressive side of the wing exceeds the detachment angle at the given Mach number or when the leading edge is too blunt, the shock is truly detached and a small region of subsonic flow is formed with a stagnation point on the high-pressure surface. As in completely subsonic cases, the flow, which cannot negotiate the turn around the leading edge, separates, overexpands, and reattaches a short distance downstream with a second shock wave.

Now consider successive plane sections of the flow parallel to the plate as the boundary layer is entered. The Mach number of the flow in successively deeper sections of the plate boundary layer decreases until the corresponding detachment angle decreases below the actual deflection angle. The roof top-wing shock wave must then detach from the leading edge and curve forward into the plate boundary layer. The flow deflection corresponding to such a shock orientation is away from the plate. Simultaneously, there is a tendency toward local bubble formation at the leading edge of the wing. While these simplified considerations cannot describe even qualitatively the complicated interaction and the resulting flow, the formation of local separated pockets is

not unlikely. The known[3] alleviation of effects on the wing from this interaction by means of a gap and numerous china-film patterns near junctures support the conjectures.

A rough study of the gap effects was included as part of the present program. A distinct streamline on the expansion side of the plate, demarking the limit of penetration of the boundary layer swept in from the compression side of the plate and wing, appears on the china-clay patterns obtained with a gap between wing and body.

In conclusion it should be observed that disturbances spreading from the leading-edge juncture are expected to modify the nonreflecting type of shock - boundary-layer interaction previously described.

C. DESCRIPTION OF MODEL

The experimental work was performed in the University of Michigan 8- by 13-inch Mach-number-1.90 channel, described in detail in reference 4. The model itself consisted of a body simulator plate and a wing which could be placed next to the body simulator plate. Figure 1 is a photograph of the model installation. Figures 2 and 3 are detailed drawings of each of the models, showing orifice locations and important dimensions. Figure 4 shows the coordinate system used in determining the position of one model with respect to the other.

The body plate may be moved parallel to itself so as to produce a gap between the wing and body plate. The wing angle of attack may be varied continuously over a range of $\pm 12°$. In addition, the wing may be rolled in order to produce various dihedral angles between the wing and the body plate. A small removable fillet on the inboard edge of the wing permits good line contact between the wing and the body plate for all dihedral angles up to 135°. The wing may be moved in an axial direction so that the orifices on the body plate may be put in various positions with respect to the leading edge of the wing.

A wire 0.031 inch in diameter was placed 1/2 inch aft of the leading edge of the body simulator plate to fix the transition point of the boundary layer on the body plate. The leading edge of the wing has a diameter of 0.005 inch at the juncture of the wing and the body, and this diameter decreases to 0.002 inch at the outboard tip.

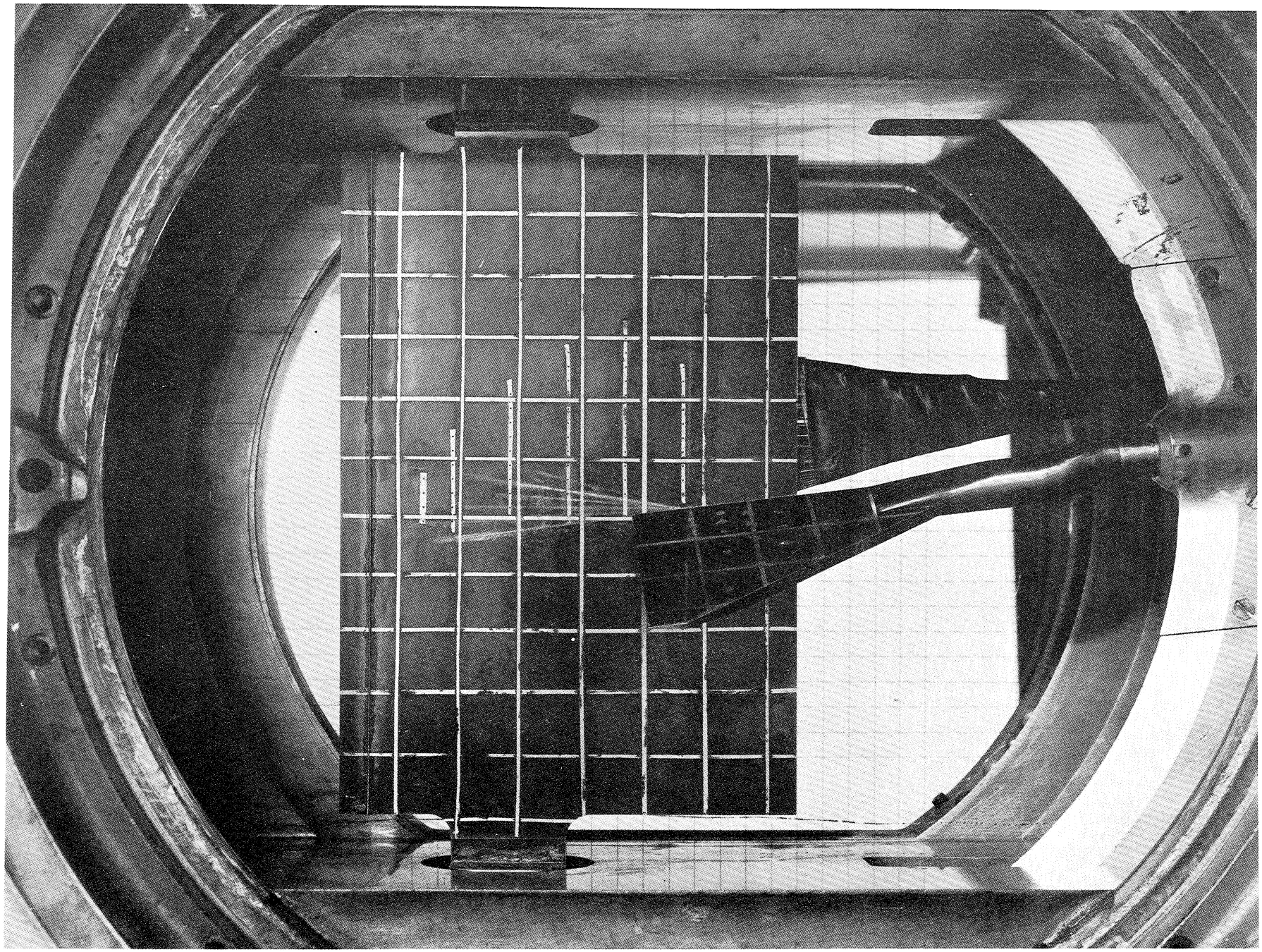

Fig. 1. Photograph of Model

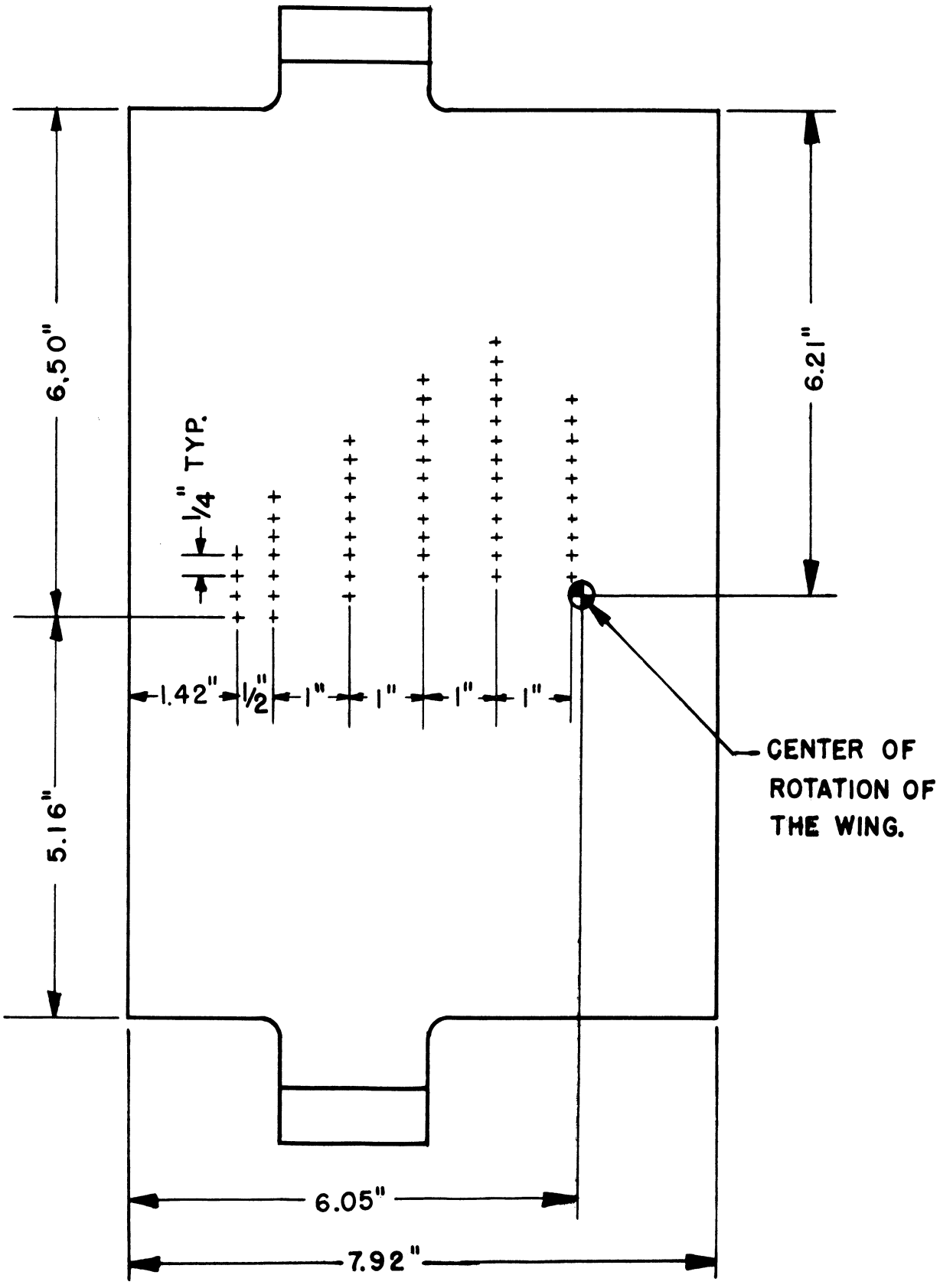

Fig. 2. Orifice Locations on Body Simulator Plate.

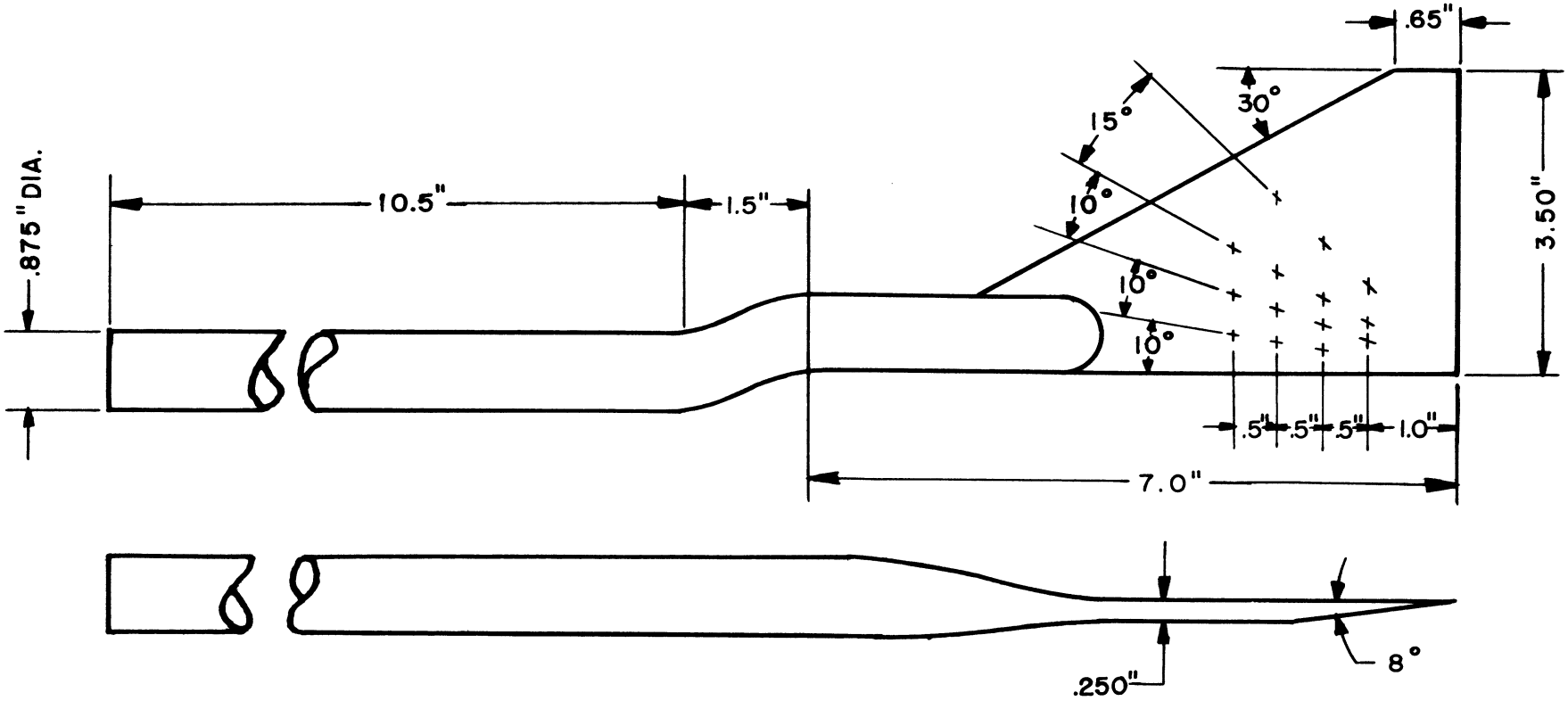

Fig.3. Orifice Locations on the Wing

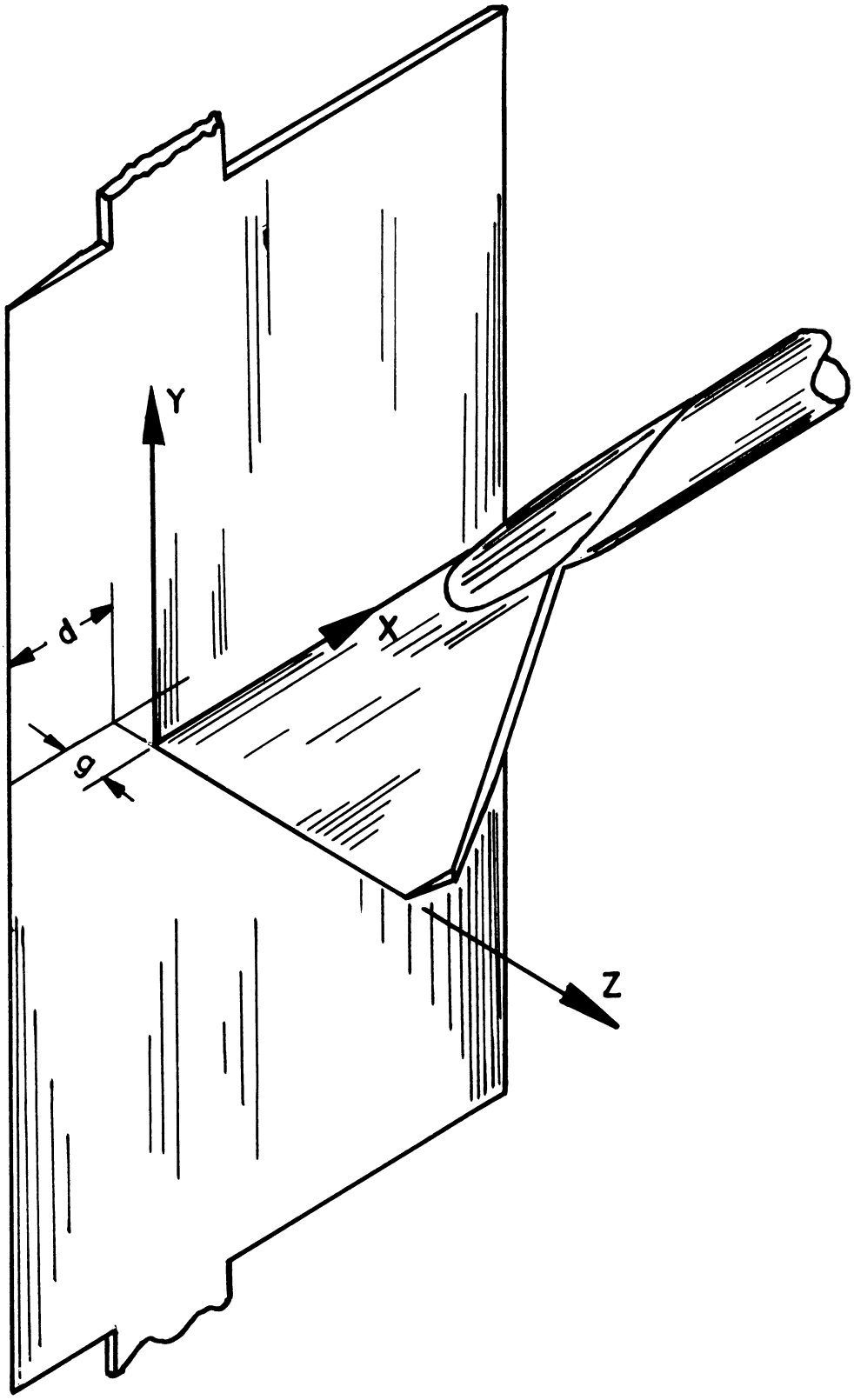

Fig. 4. Coordinate System

D. REDUCTION AND PRESENTATION OF DATA

The pressure orifices on both models were connected to mercury manometers which were photographed during each run in order to record the pressures measured at the orifices. The reduction of all pressure data to the form p/p_b (ratio of static pressure measured at the orifice to barometric pressure) permits the comparison of data taken from different runs, since the barometric pressure, p_b, is identical to the stagnation pressure, p_o, for all practical purposes.

The effect of tunnel nonuniformities on the data obtained from this model is quite different from their effect on the data obtained from the cylindrical wing-body interaction model presented in reference 1. The orifices on the body plate are fixed with respect to the wind tunnel. Thus, as long as the tunnel nonuniformities are fixed with respect to the tunnel, a simple subtraction of the pressure ratios measured on the flat plate alone from the pressure ratios measured on the flat plate in the presence of the wing should serve to eliminate the effects of these nonuniformities. Actually, computations show that a Mach wave passing through the region affected by the wing may impinge on the body plate as much as 1.2 inches forward of its point of impingement in the absence of the wing, if the wing angle of attack is -8°. Therefore, it is possible that a tunnel nonuniformity may affect a certain orifice on the body plate in the absence of the wing and not affect this same orifice when the body plate is in the presence of the wing. The data obtained from this orifice will then be slightly inconsistent with the data obtained from another orifice which is in the same relative position with respect to the wing, but which is completely unaffected by the tunnel nonuniformity. No systematic method of correcting this type of error could be devised so that it is necessary in examining the experimental results presented in this report, which were obtained by the simple subtraction of body-alone pressures from body pressures measured in the presence of the wing, to keep in mind the fact that slight inconsistencies of the above type may occur.

The manner in which the data are plotted varied depending on the configuration tested.

E. DISCUSSION OF EXPERIMENTAL RESULTS

The configurations tested may conveniently be broken down into three categories. First are the configurations in which the effects of angle of

attack of the wing on the body plate pressures were investigated. In the second category the dihedral angle between the wing and the body plate was varied. In the last group of configurations there was a gap between the wing and the body plate.

1. Angle-of-Attack Effect

A negative angle of attack occurs when a shock wave at the leading edge of the wing causes the pressure on the flat surface of the wing to be greater than ambient.

The effect of angle of attack on the static pressures measured on the body simulator plate is shown in Figs. 5 and 6, which are plots of $\Delta p/p_o$ versus x. $\Delta p/p_b$ is the ratio of the difference between the static pressure measured on the body alone and the static pressure measured on the body in the presence of the wing to the stagnation pressure. The standard deviation of the experimental pressure data is $\sigma\Delta p/p = \pm 0.0020$. This value includes small variations in the angle of attack of the wing as well as the inaccuracy of the mercury manometers used to measure the static pressure. The value of y associated with each pressure profile is the distance from the plane of the wing to the orifice row in question when the wing leading edge is 2 inches aft of the leading edge of the body plate, i.e., when d = 2 inches in Fig. 4.

As the wing is moved axially, each orifice on the body plate will trace out a pressure curve. Since the rows of orifices on the body plate are parallel to the undisturbed flow upstream of the wing while the wing moves parallel to itself in a plane which makes an angle α_w with the free stream, the segments of the pressure curves traced out by two orifices, one behind the other, will not match at their end points. Therefore, in order to obtain a continuous pressure profile it is necessary to pick some position of the wing with respect to the body as a standard and then correct all other positions to agree with this position. Such a correction merely amounts to a slight shift in the axial position of the pressure points, the amount of the axial shift being greater for those axial positions of the wing which are farther from the standard position. The assumption that the pressure is constant along Mach lines approximately parallel to the shock wave from the leading edge of the wing is inherent in this correction method. The resulting curve then represents a pressure profile which is parallel to the free stream ahead of the leading edge of the wing and at a distance y above the leading edge of the wing.

The experimental pressure profiles in Figs. 5 and 6 have been treated in this manner. In Fig. 6 the theoretical pressure profiles, which can be obtained from Prandtl-Meyer flow and simple shock-wave theory, are shown together with the experimental pressure profiles. Pressure profiles are available only

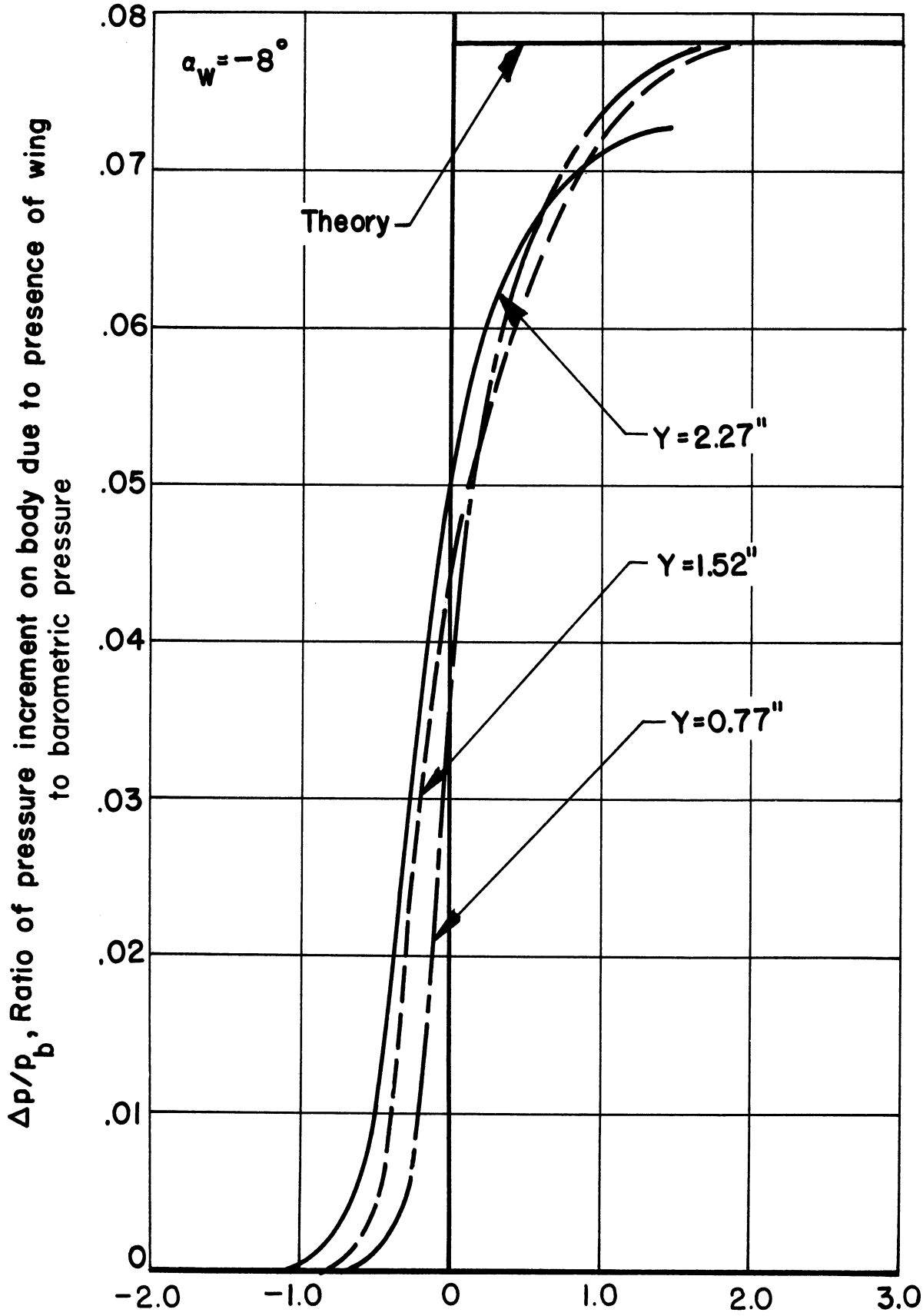

Fig. 5a. Axial pressure curves for various values of y.

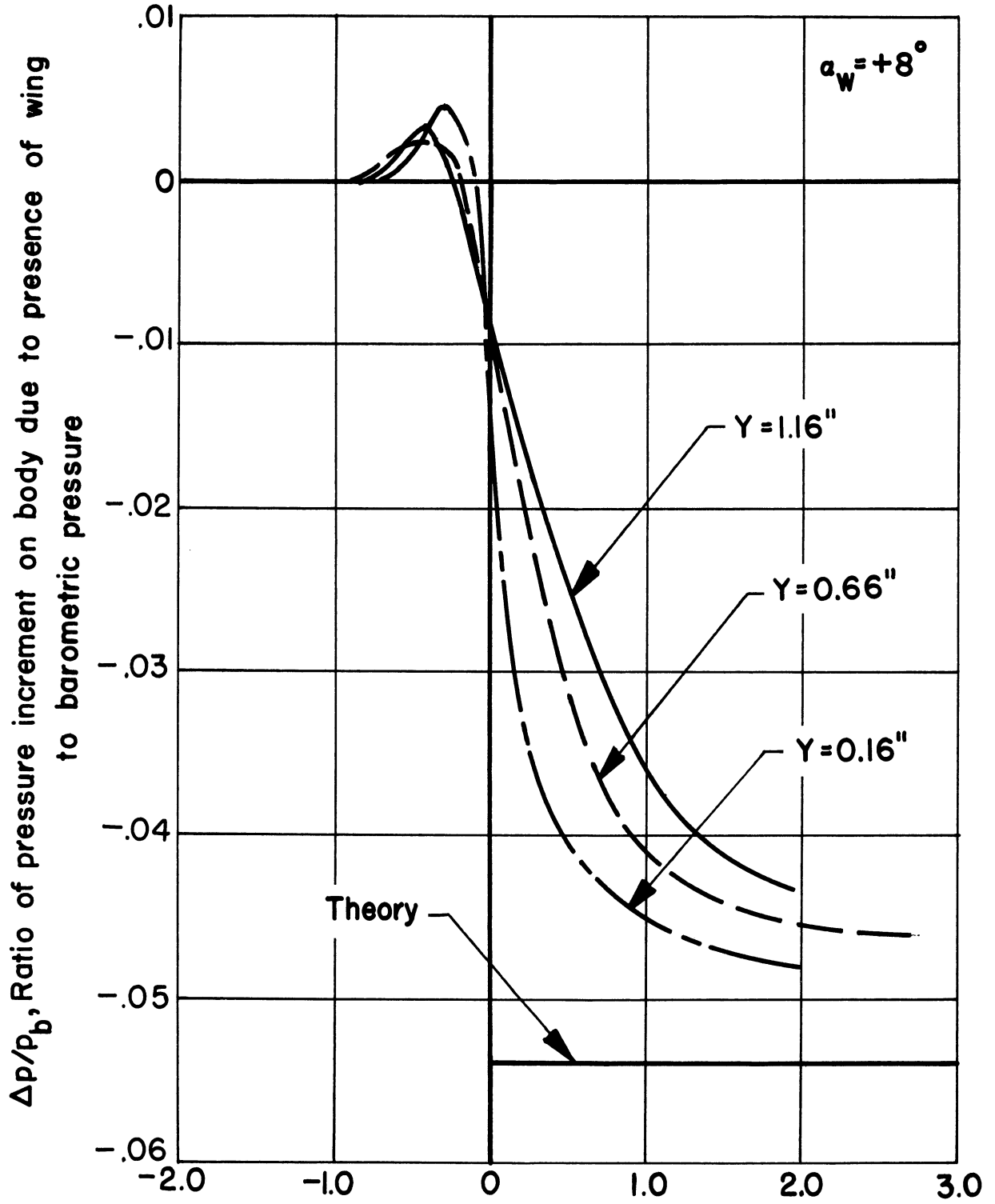
.01
0
-.01
-.02
-.03
-.04
-.05
-.06
-2.0
-1.0
0
1.0
2.0
3.0
$a_w = +8°$
Y = 1.16"
Y = 0.66"
Y = 0.16"
Theory
$\Delta p/p_b$, Ratio of pressure increment on body due to presence of wing to barometric pressure
Axial distance in inches from the theoretical position of the first Mach wave in the Prandtl-Meyer expansion

Fig. 5b.

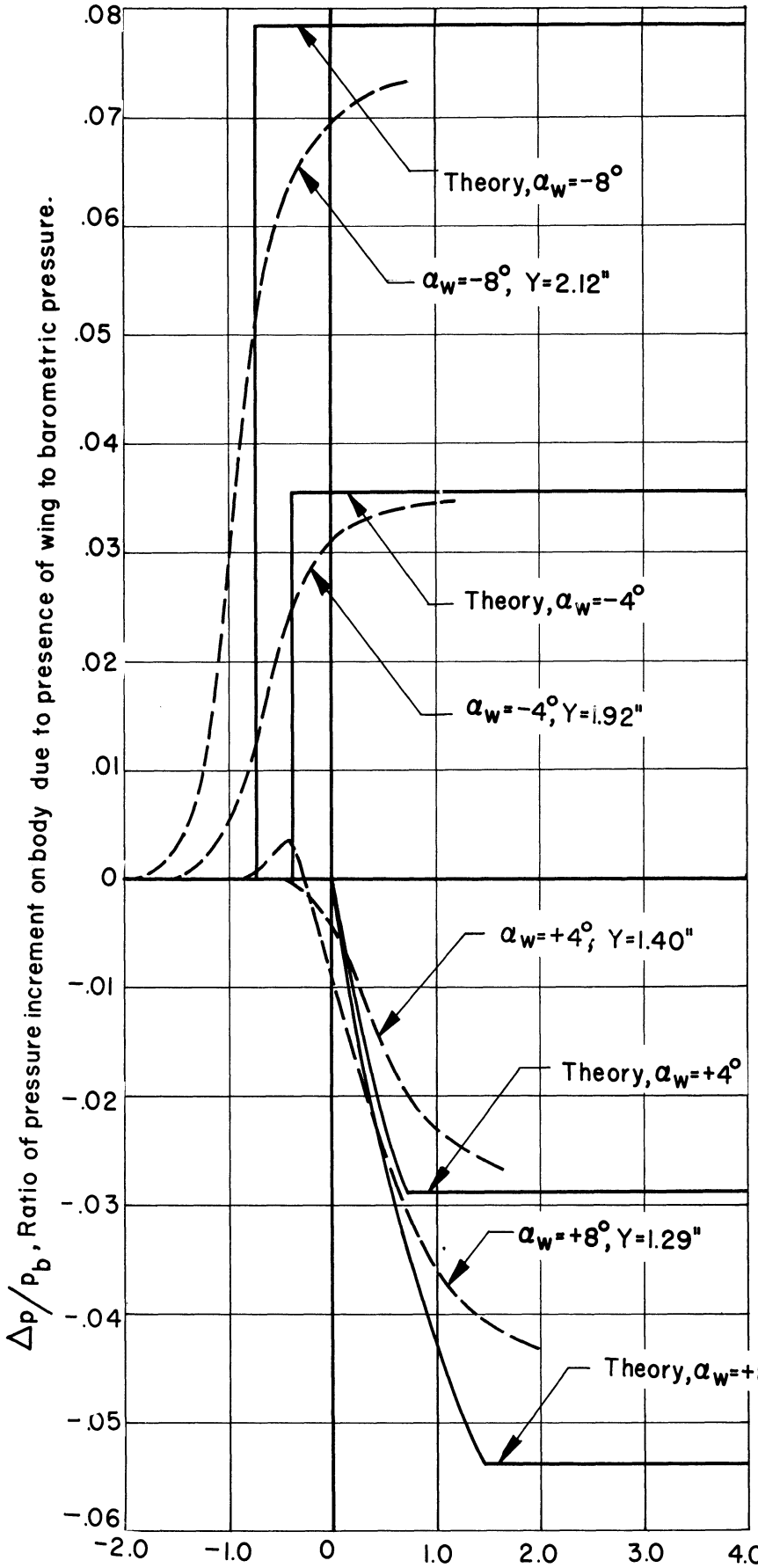

Fig. 6a – Axial pressure curves for various values of α_w.

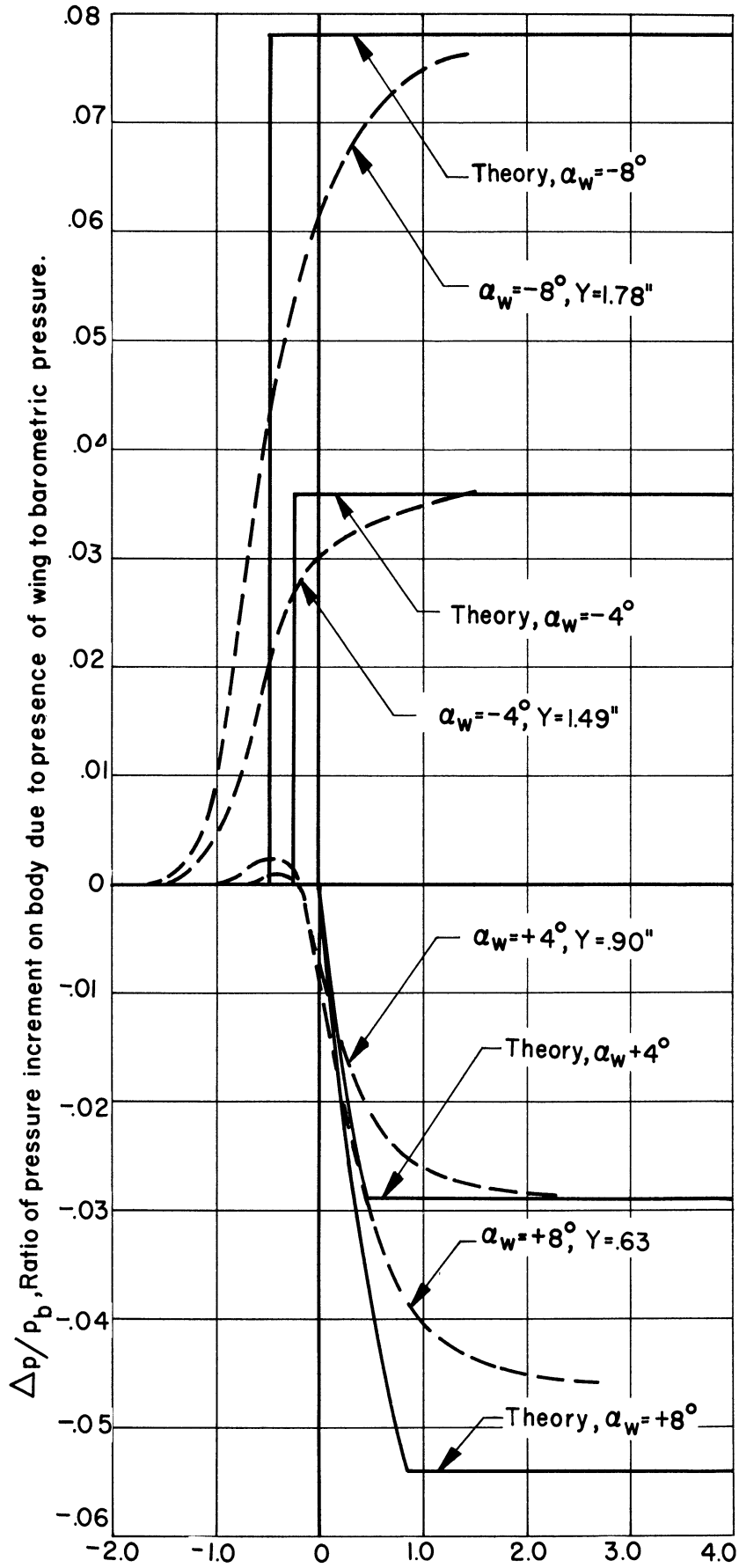
.08
.07
.06
.05
.04
.03
.02
.01
0
-.01
-.02
-.03
-.04
-.05
-.06
-2.0
-1.0
0
1.0
2.0
3.0
4.0
Theory, α_w=-8°
α_w=-8°, Y=1.78"
Theory, α_w=-4°
α_w=-4°, Y=1.49"
α_w=+4°, Y=.90"
Theory, α_w+4°
α_w=+8°, Y=.63
Theory, α_w=+8°
$\Delta p / p_b$, Ratio of pressure increment on body due to presence of wing to barometric pressure.
Axial distance in inches from the theoretical position of the first Mach wave in the Prandtl-Meyer expansion.

Fig. 6b

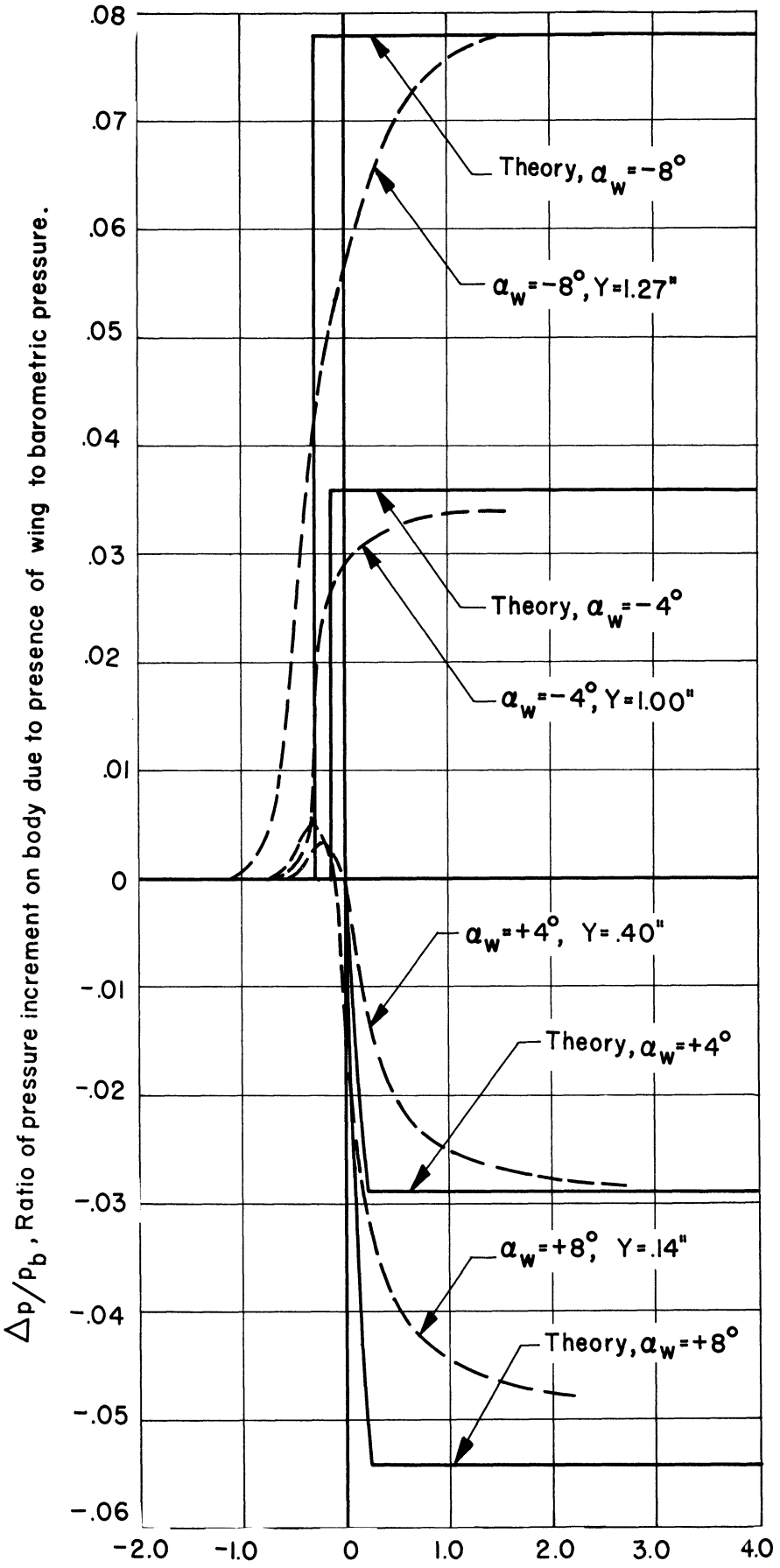

Axial distance in inches from the theoretical position of the first Mach wave in the Prandtl-Meyer expansion.

Fig. 6 c

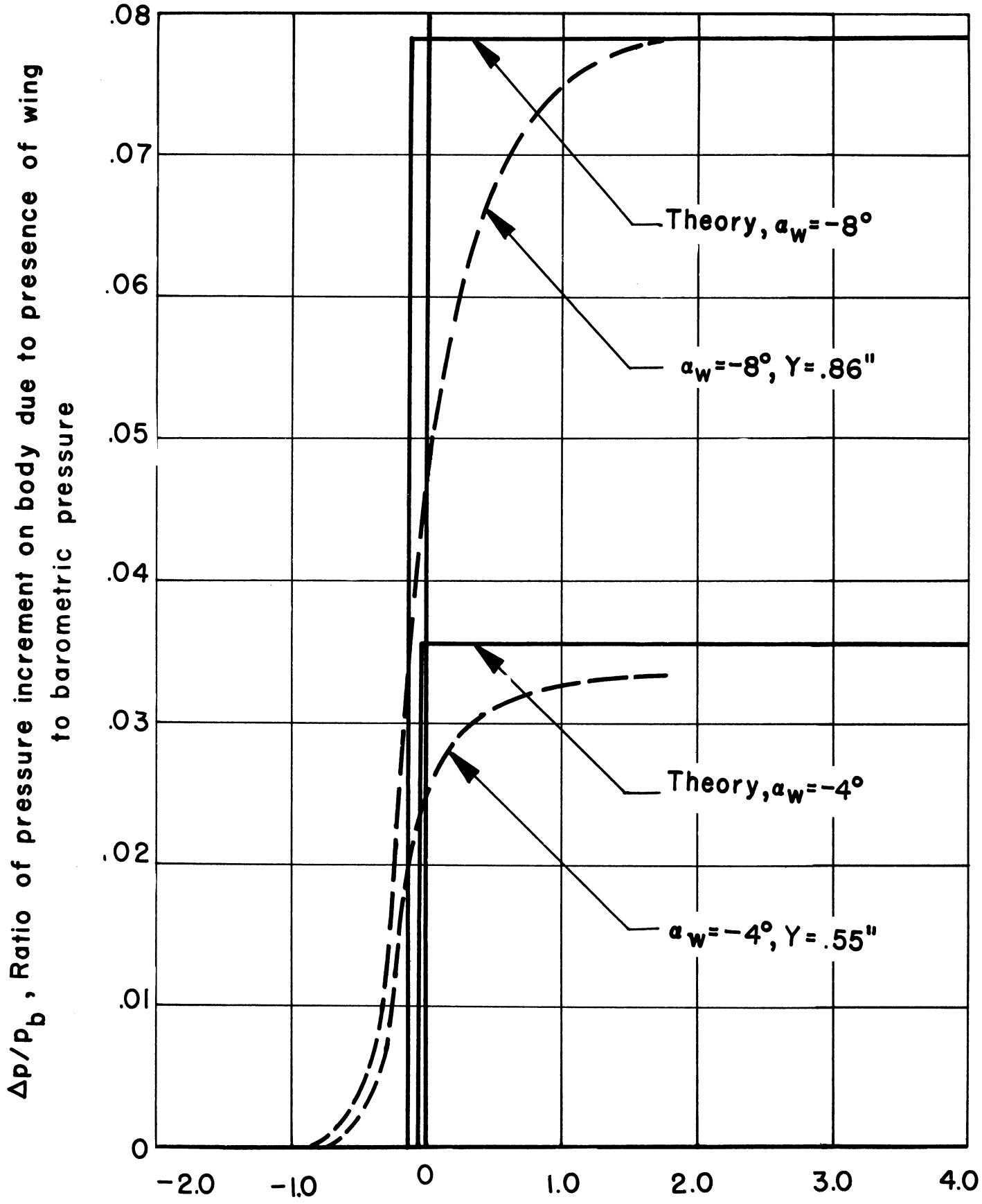

Axial distance in inches from the theoretical position of the first Mach wave in the Prandtl-Meyer expansion.

Fig. 6d

for α_w = -8 and -4° in Fig. 6d, since this row of orifices was below the wing for α_w = +4 and +8°. It is apparent that for these small values of y the experimental pressure rise begins about 0.7 inch ahead of the theoretical pressure rise, and reaches the theoretical post-shock-wave value 1 inch aft of the theoretical jump position for α_w = -4° and 1.5 inches aft for α_w = -8°. Examination of the pressure profiles in Fig. 5 shows that with increasing y the amount of forward propagation increases up to 1.2 inches, for y = 2.27 α_w = -8°. At the same time the experimental curves take longer to reach the theoretical post-shock value. This means that as one proceeds out along the intersection of the wing shock wave and the body plate, the pressure rise is continually softened. This softening effect is caused by the increasing thickness of the boundary layer on the body plate, which is due to the increased distance aft of the leading edge of the body and to the crossflow of the air in the boundary layer on the body.

For positive angles of attack the pressure profiles clearly indicate that a weak shock wave precedes the expansion wave as mentioned in section B.

In addition to the axial pressure profiles discussed above the data have been plotted in conical coordinates. A pecularity of the conical coordinate system used in these plots of the experimental data is that for those points associated with a small value of x any deviation of the actual flow from the theoretical conical flow will be greatly magnified. Conversely, for large values of x any deviation of the actual flow from the theoretical conical flow will be diminished so that the deviation may be masked by the experimental scatter of the data. It is important when examining the data to keep this property of the conical coordinate system in mind. For instance, those experimental points associated with small values of x may be expected to differ considerably from their theoretically predicted values, since for a given value of $\beta r/x$, r and x become small together, and when they approach the order of magnitude of the boundary-layer thickness the flow will be strongly affected by the leading-edge bluntness, the buildup of the boundary layer on the wing, and the interaction between the shock wave at the leading edge of the wing and the boundary layer on the body plate. In Fig. 7 C_p/C_{p_o} is plotted versus $\beta r/x$ for $\alpha_w = \pm 4, \pm 8°$. C_p is the experimentally measured value of the pressure coefficient, C_{p_o} is the value of the pressure coefficient predicted by linearized theory, β is the cotangent of the Mach angle, x is in the streamwise direction, and $r = \sqrt{y^2 + z^2}$ (see Fig. 4). Two theoretical curves are also included in Fig. 7 for each value of α_w. The first theoretical curve is the one given by linearized theory while the second is the one given by exact theory, i.e., simple shock-wave theory or Prandtl-Meyer flow theory. The experimental points measured on the body have been plotted with different symbols according to the values of x and d associated with each point. The experimental points measured on the wing have been plotted with different symbols according to the value of x associated with each point. The values of the wing pressure coefficients which are plotted in Fig. 7 are actually the averages of

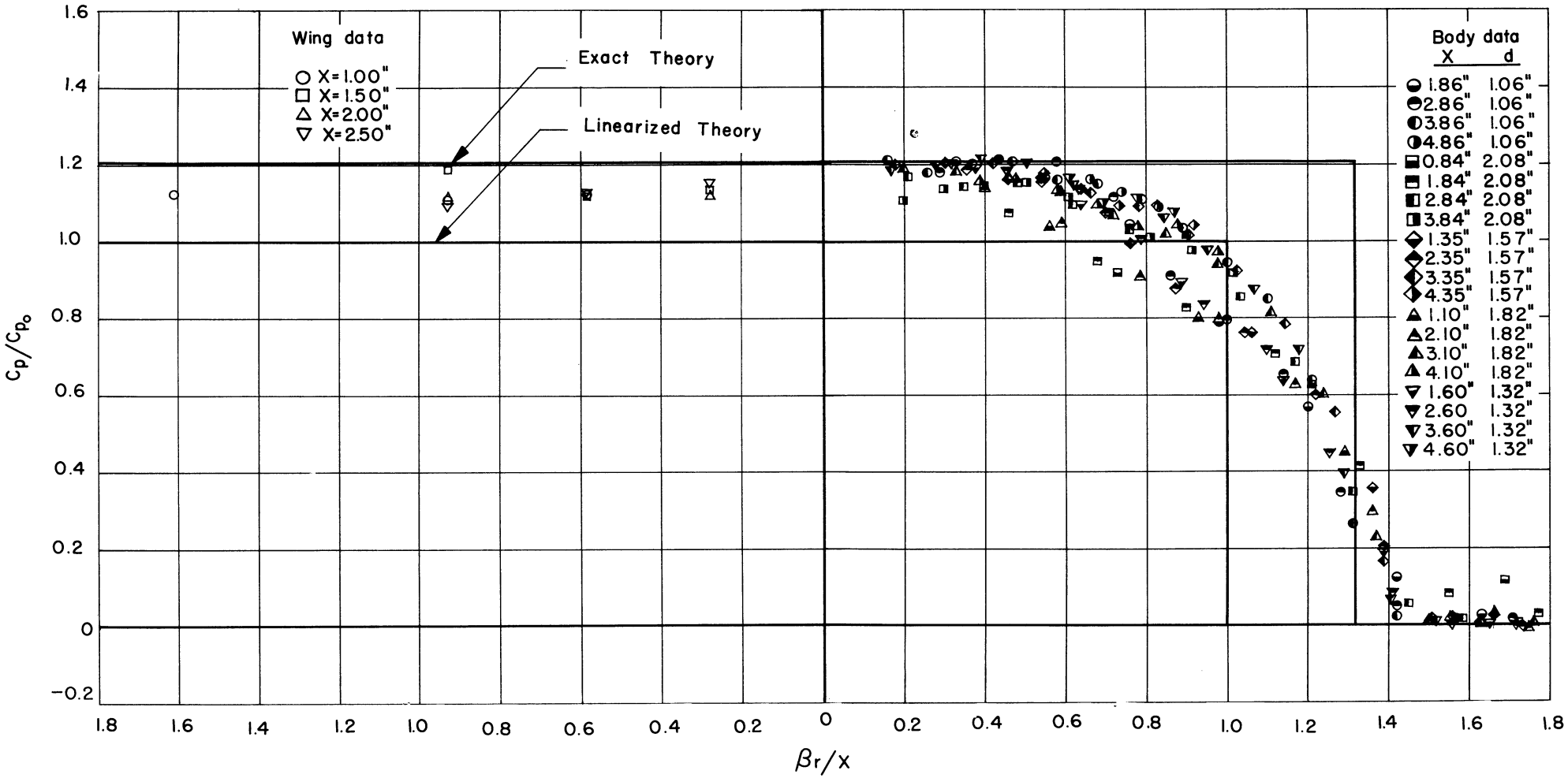

Fig. 7a– Experimental data in conical coordinates: zero gap, ϕ=90°, α_w=−8°.

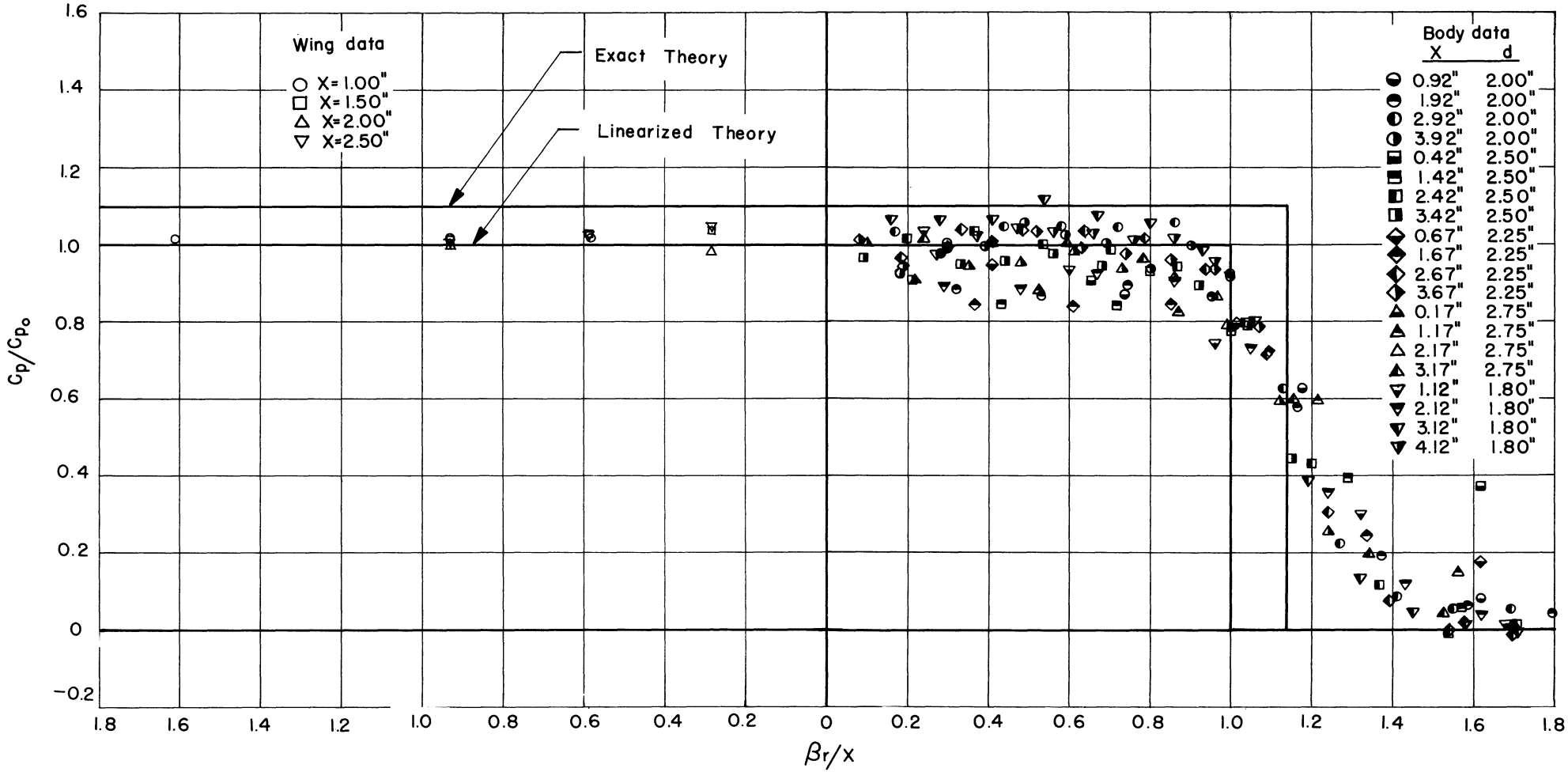

Fig. 7b—Experimental data in conical coordinates: zero gap, $\phi=90°$, $\alpha_w=-4°$.

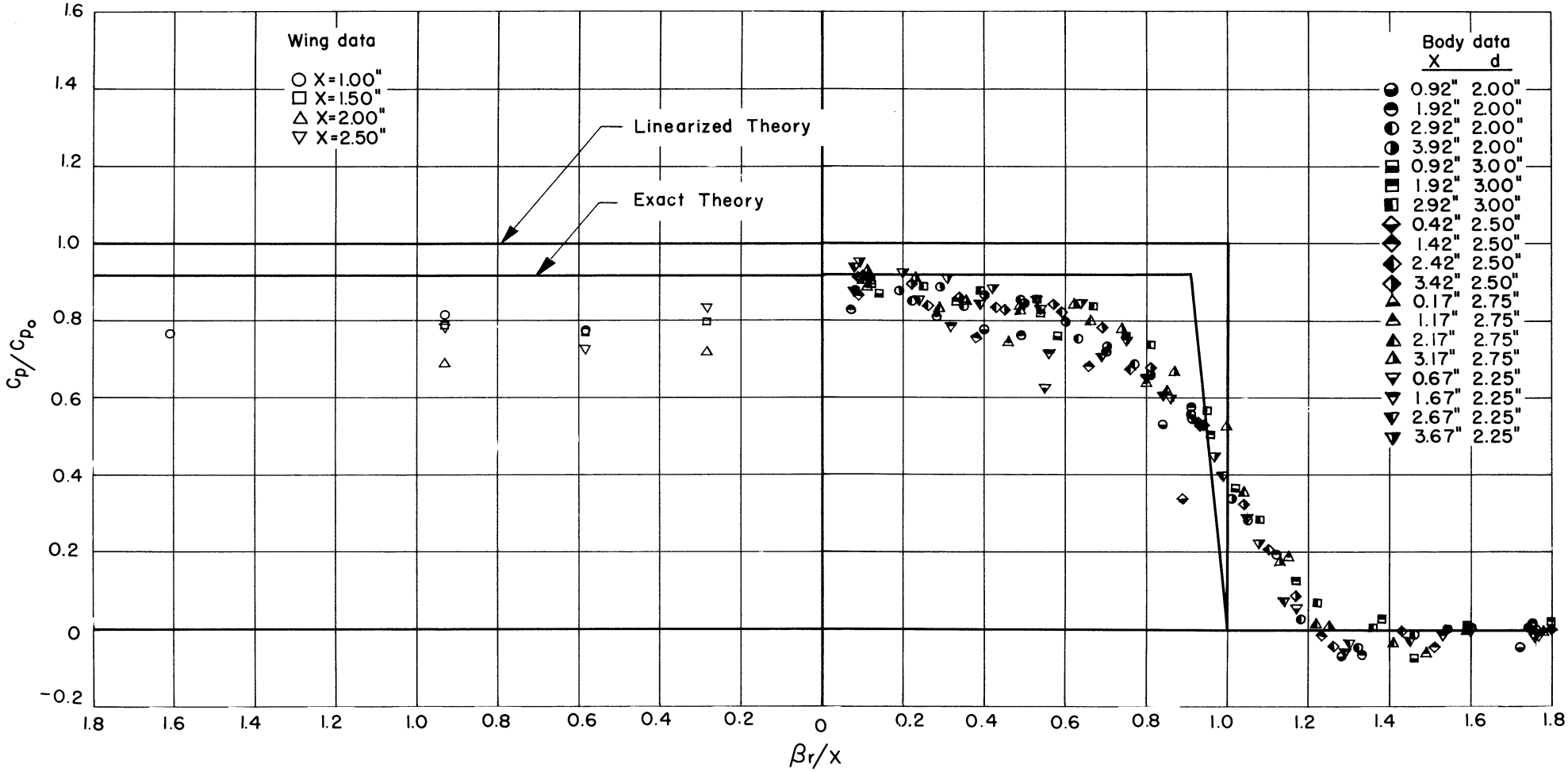

Fig. 7c — Experimental data in conical coordinates: zero gap, $\phi = 90°$, $\alpha_w = +4°$.

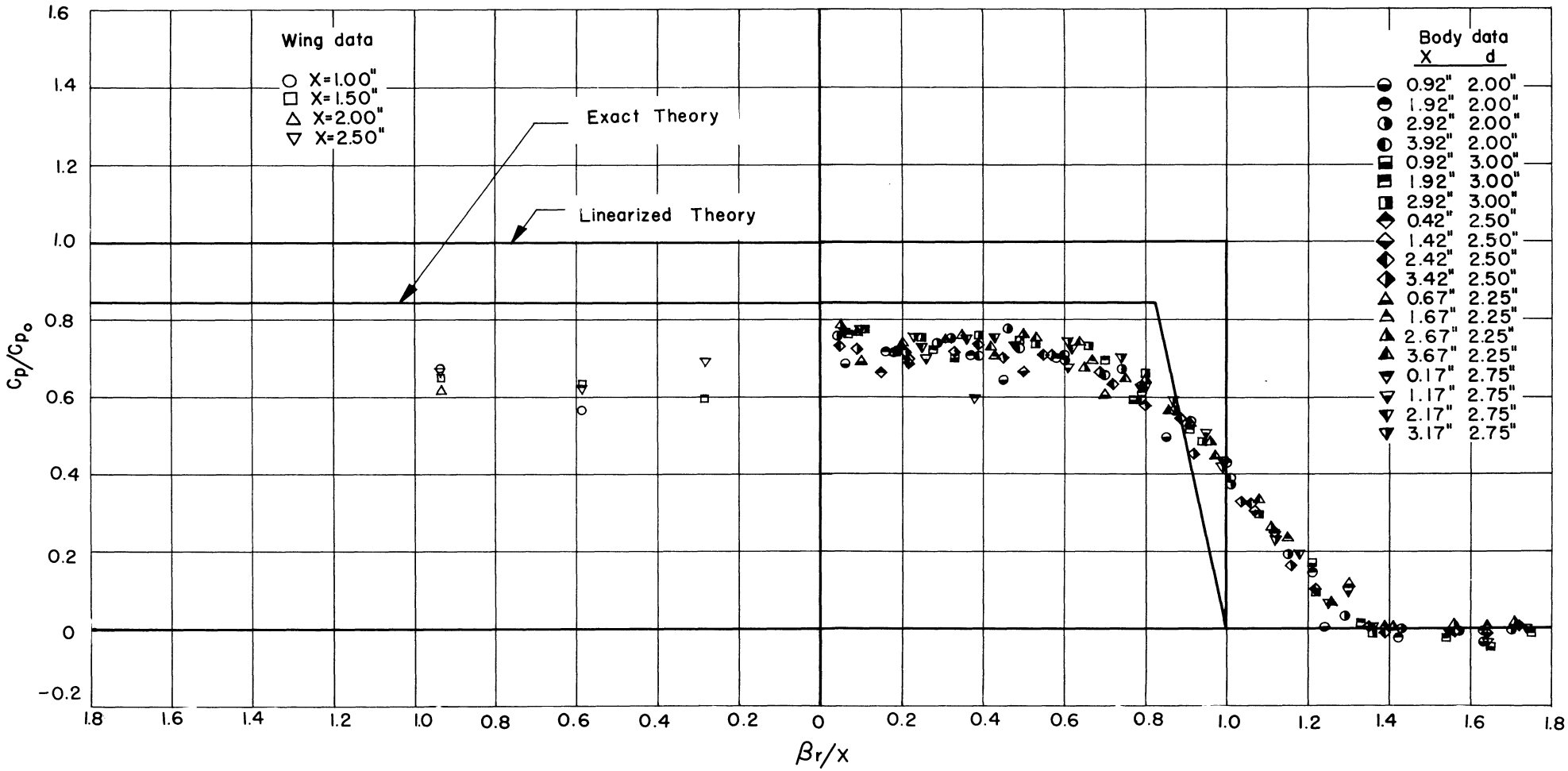

Fig.7d – Experimental data in conical coordinates: zero gap, $\phi = 90°$, $\alpha_w = +8°$

several values recorded for different values of d, since a variation in d does not affect the static pressures measured on the wing within the experimental accuracy. This independance of the static pressures measured on the wing from the value of d implies that the interaction phenomena occurring on the wing are insensitive to the thickness of the boundary layer on the body.

a. $\alpha_w = -8°$. Figure 7a presents the experimental points for -8° angle of attack of the wing. All the points for which $2.5 \leq x \leq 4.0$ fall on one curve, which indicates that the flow is apparently conical in this region. However, for values of $x \leq 2.5$ the experimental points are consistently below this curve behind the wing shock wave and consistently above this curve ahead of the wing shock wave. Therefore, it appears that as x increases the experimental points tend toward a limit curve, indicating that while the flow is definitely not conical near the leading edge of the wing it may become conical farther aft. This nonconicity of the flow near the leading edge of the wing is due to the effect of the boundary layers on the wing and the body together with the finite thickness of the leading edge of the wing as discussed earlier.

An examination of Fig. 7a shows that some of the points which lie below the limiting curve appear to define a second, lower curve quite distinct from the limiting curve. It is possible that the tunnel shocklets which are known to be present shift so much in the presence of the wing that the zero pressures become incorrect as mentioned in section D. The observed experimental pressure jump is larger than that predicted by linear theory but is in good agreement with the value predicted by simple shock-wave theory. The major portion of the pressure rise occurs in the region $0.55 \leq \beta r/x \leq 1.55$, the pressure rise beginning slightly ahead of the position which is indicated by simple shock-wave theory.

The pressures measured on the wing are slightly below the value predicted by shock-wave theory.

b. $\alpha_w = -4°$. The trend toward a limit curve as x increases is evident in Fig. 7b, which shows the results obtained for -4° angle of attack. In this case the trend is masked somewhat by an increase in the random scatter of the experimental points. This increase in the apparent random scatter of the data is due to the smaller value of C_p predicted by the linear theory in the case of -4° angle of attack.

The experimentally measured pressure jump is 10 percent short of the value predicted by exact shock-wave theory. The position of the pressure jump is again ahead of the position predicted by shock-wave theory. The major portion of the pressure rise occurs in the region $0.80 \leq \beta r/x \leq 1.55$.

c. $\alpha_w = +4°$. The results obtained for an angle of attack of the wing of +4° are shown in Fig. 7c. The same tendency for the experimental

points to approach a limiting curve appears for this angle of attack. For values $x \gtrsim 1.5$, the flow appears to be conical. The shock wave which precedes the Prandtl-Meyer expansion at the leading edge of the wing does not appear sharply on this plot as it did on the axial pressure profiles. There are two reasons for this behavior, the first being the tendency of the bump to be smeared out because of the conical transformation which is less accurate for small values of x. The second reason is that the shocklet will affect the static pressure orifices only for certain values of the distance d, and not all the values of d which were tested are presented in the plots of Fig. 7c, whereas the faired results of Figs. 5 and 6 include all of the test results for certain rows of orifices.

The measured pressure drop is 86 percent of the value predicted by linear theory and 93 percent of the value predicted by exact theory, i.e., the Prandtl-Meyer flow. The major portion of the pressure drop occurs in the region $0.6 \leq \beta r/x \leq 1.3$.

The static pressures measured on the wing are lower than the average static pressures measured on the body plate, well behind the Prandtl-Meyer flow from the leading edge of the wing. The average value of the pressure coefficient on the wing is about 80 percent of the value predicted by exact theory.

d. $\alpha_w = +8°$. The experimental results plotted in Fig. 7d are for an angle of attack of the wing equal to +8°. The same trend as that which occurred at the other angles of attack is present in these data although most of the experimental points are for larger values of x.

The pressure drop is 86 percent of the value predicted by exact theory and 72 percent of the value indicated by linear theory. The major portion of this pressure drop occurs in the region $0.65 \leq \beta r/x \leq 1.35$.

The pressure coefficients recorded on the wing are about 65 percent of the value predicted by linear theory and 77 percent of the value predicted by exact theory.

2. Dihedral Effect

Tests were made at both +8 and -8° angle of attack with wing dihedral angles of 45 and 135°. The experimental results are shown in Fig. 8 as plots of C_p/C_{p_o} versus $\beta r/x$. The same scheme has been used for labeling the experimental points as was used in Fig. 7; i.e., a different symbol is used for each value of x and d. The linearized theory for the dihedral angle of 135°, which is also shown in Fig. 8, was obtained from reference 5. For a dihedral angle of 45° the theoretical curve may be obtained using the method presented in

reference 6. With the wing in the rolled position, i.e., for dihedral angles of 45 and 135°, the flow is not deflected through 8° when the wing angle of attack is set at 8°. The true flow deflection when the wing is set at 8° angle of attack in the rolled position is 5.67°. Thus, C_{p_o} in this case is the pressure coefficient predicted by linearized theory for 5.67° of flow deflection.

The results obtained for the wing at -8° angle of attack and a dihedral angle of 135° are shown in Fig. 8a. The experimental points are again labeled with their proper values of x and d and presented in terms of C_p/C_{p_o} versus $\beta r/x$. The agreement of these experimental points with the theory of reference 5 is especially good for larger values of x. The pressure rise begins somewhat ahead of the point predicted by the linearized theory. The pressures measured on the wing also agree well with their theoretically predicted values.

Figure 8b shows the results obtained for a dihedral angle of 135° when the wing is at +8° angle of attack. It is evident that the flow is not conical. The compression which occurs in the range $1.3 \leq \beta r/x$ is probably the continuation of the shock wave which occurs on the lower surface of the wing. The extent of this shock is considerably magnified in the conical coordinates. The depth of this dip varies from $C_p/C_{p_o} = 0.35$ at x = 1 inch to $C_p/C_{p_o} = 0.2$ at x = 3 inches. These values of C_p/C_{p_o} correspond to a shock wave with a flow deflection of 1.5 to 2°. The experimental points show a very definite trend in the region $1.8 \geq \beta r/x \geq 1.4$, where the pressure increases for a fixed value of $\beta r/x$ with a decreasing value of x. In the region $\beta r/x \leq 0.5$ a recompression occurs which appears to be stronger for smaller values of x.

A possible cause of the pressure variations described in the preceding paragraph is the local detachment of the shock wave at the leading edge of the wing due to the combined effects of (1) the bluntness of the leading edge of the wing, (2) the large angle of attack on the lower surface of the wing, and (3) the choking effect of the channel formed by the body plate and the lower surface of the wing. This local detachment may then be accompanied by the familiar bubble on the upper surface at the leading edge of the wing. The resulting shock-expansion-shock configuration could then hardly be expected to be conical, especially for the smaller values of x.

The pressures measured on the wing for this configuration lie considerably below the value predicted by linearized theory. The pressured recorded on the wing outside the Mach cone are approximately one half of the value predicted by linearized theory.

The experimental results shown in Fig. 8c apply to the case of a 45° dihedral angle between the wing and the body plate with the wing at -8° angle of attack. The pressures measured on the body rise to a higher value than that

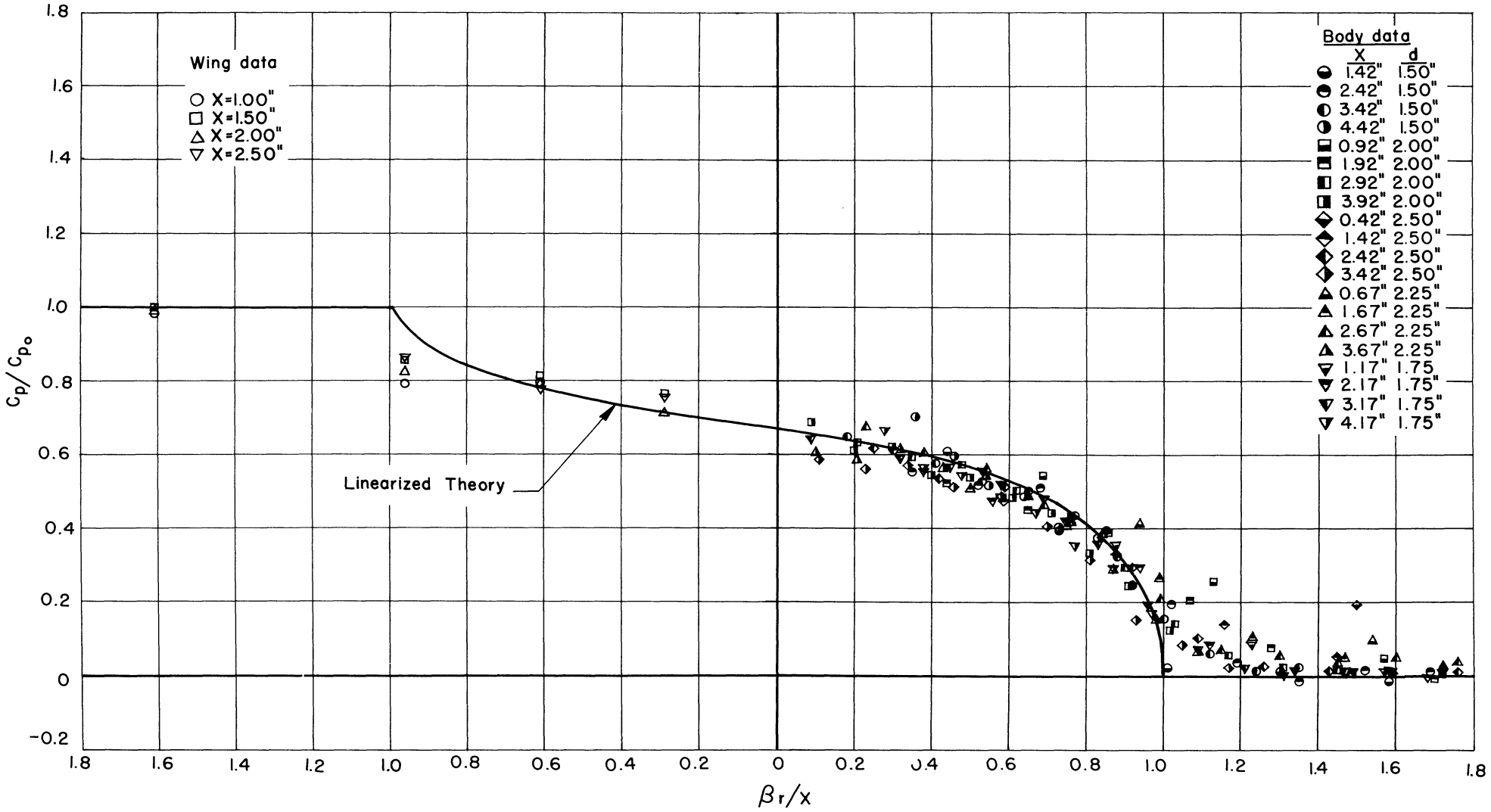

Fig. 8a – Experimental data in conical coordinates: zero gap; ϕ=135°, α_w=-8°.

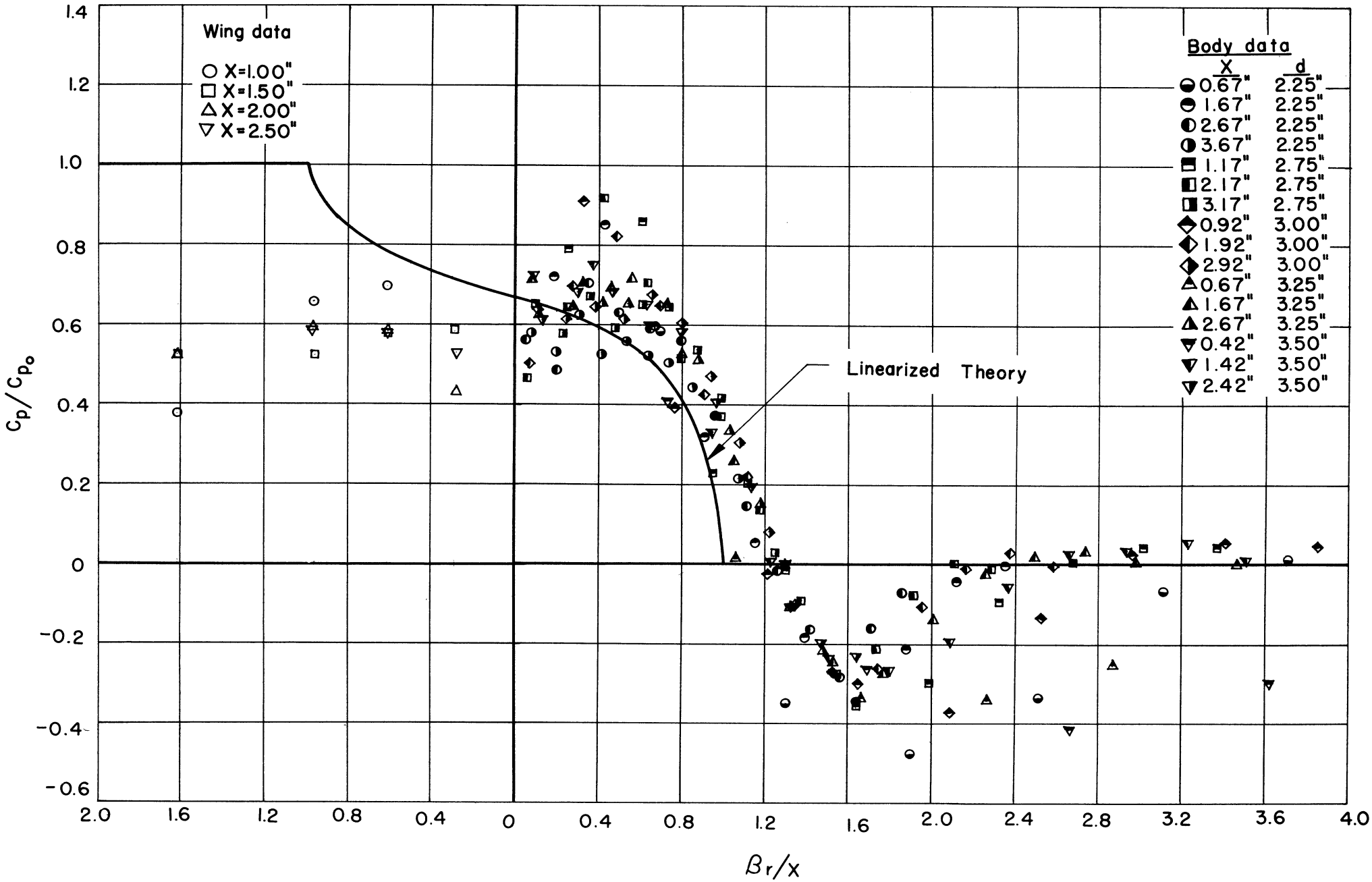

Fig. 8b— Experimental data in conical coordinates: zero gap, ϕ=135°, α_w=+8°

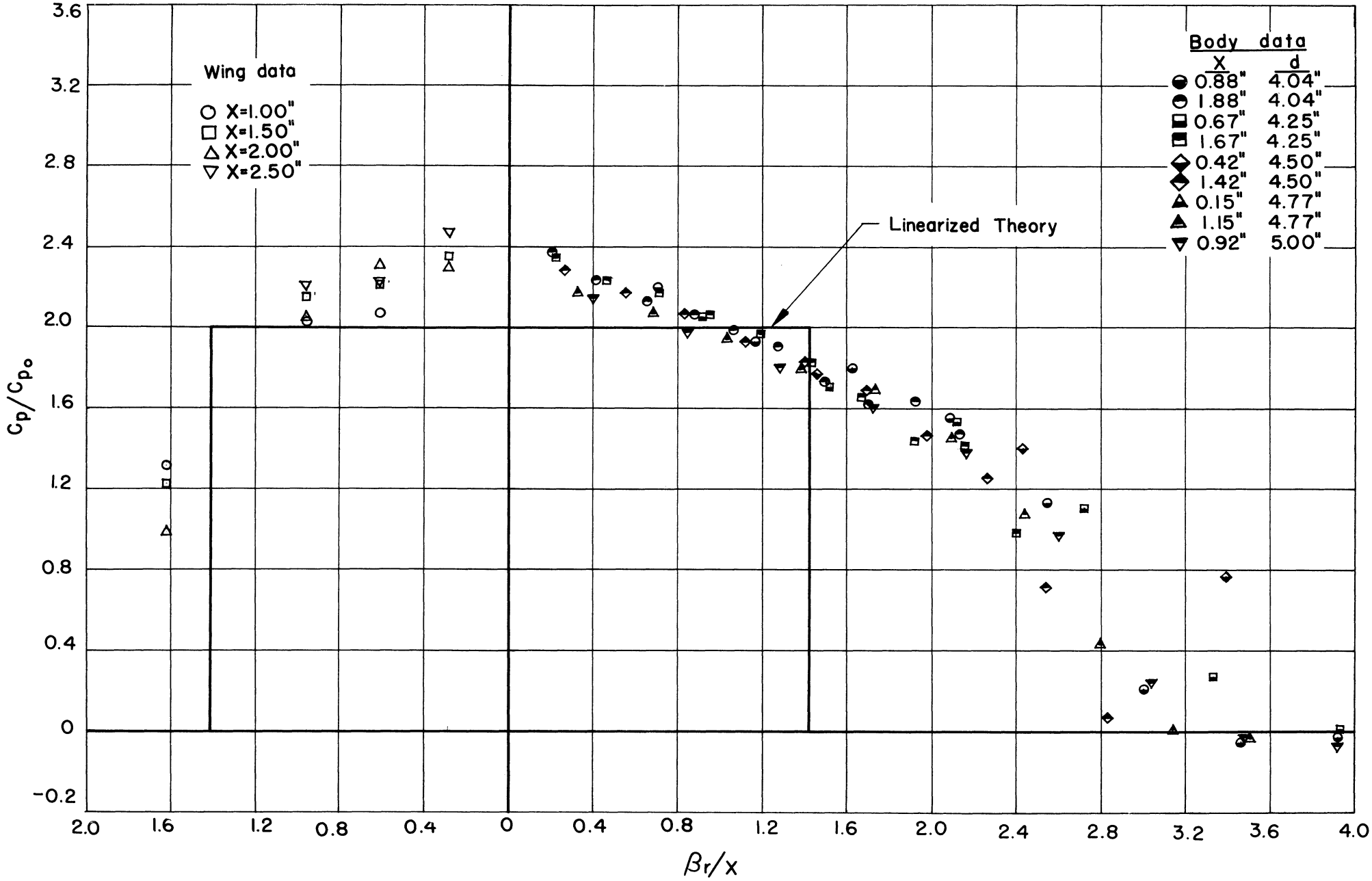

Fig.8c— Experimental data in conical coordinates:zero gap, ϕ=45°, α_w=−8°.

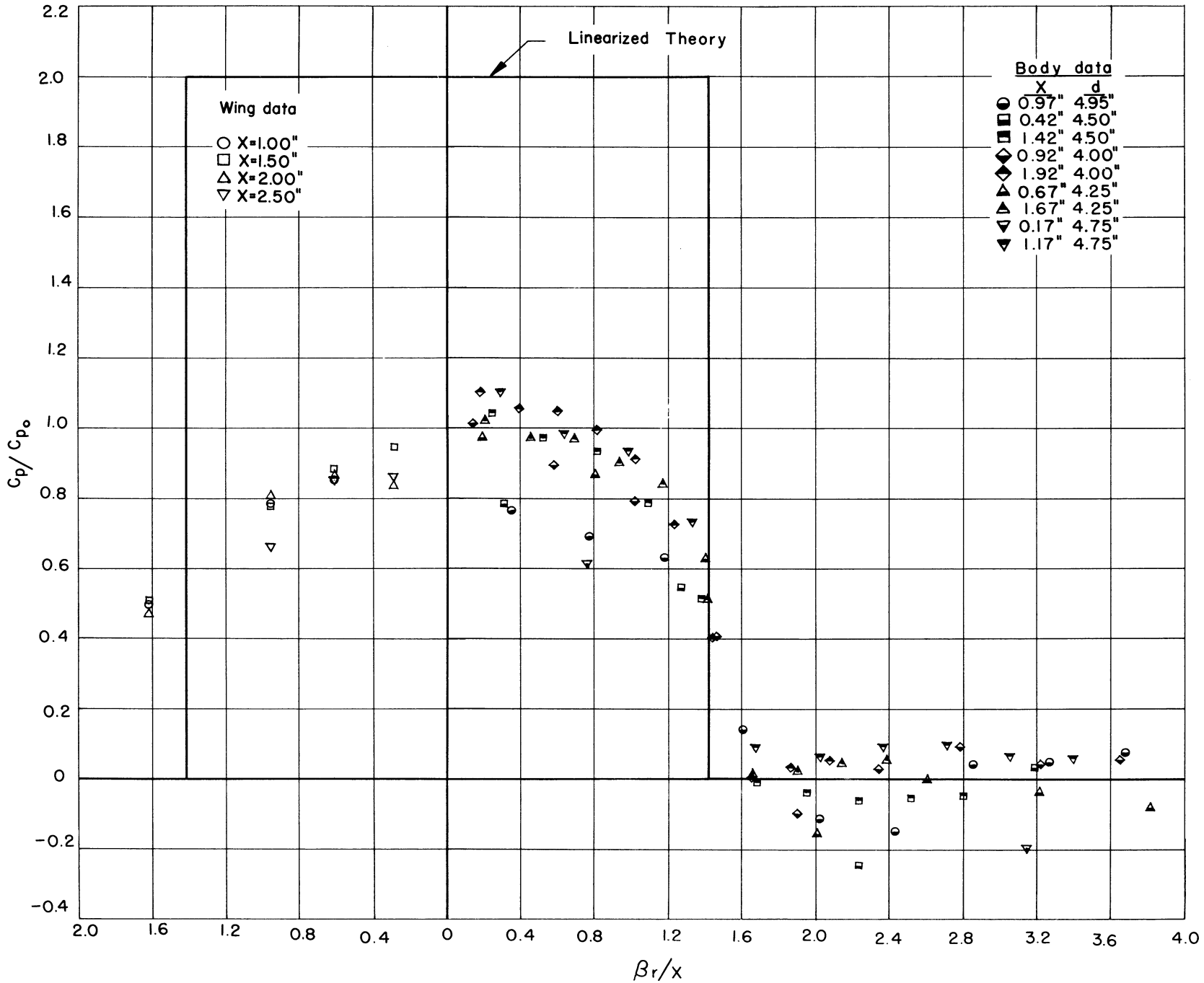

Fig.8 d – Experimental data in conical coordinates: zero gap, $\phi = 45°$, $\alpha_w = +8°$

predicted by linearized theory. The pressure rise begins considerably before the point indicated by linearized theory. The shock-wave angle measured with the china-clay film technique was $\theta_w = 48°$. This value of θ_w corresponds to $\beta r/x = 2.53$, and a glance at Fig. 8c shows that the pressure rise does indeed commence at or slightly ahead of this value of $\beta r/x$. The experimental points associated with low values of x are higher than those for high values of x in the region $\beta r/x > 2.5$.

The pressures measured on the wing are higher than would be expected on the basis of linearized theory.

The experimental data presented in Fig. 8d apply to the case of +8° angle of attack of the wing and a dihedral angle of 45°. There is again a shock wave preceding the Prandtl-Meyer flow at the leading edge of the wing. For values of $x > 1.0$ inch the shock wave is not present. At $x = 0.42$ the shock wave is strongest; giving a flow deflection of about 1.5° The experimental points for this case are considerably below the values predicted by theory. The pressures tend to be low for small values of x. For $x > 1.0$ inch the flow appears to be conical and all points, no matter what their value of x, fall on the same curve.

On the wing the experimental points are considerably below the linearized-theory curve. Near the juncture the value of C_p/C_{p_o} on the wing is approximately 1, but outside the Mach cone from the juncture of the leading edge of the wing and the body plate the value of C_p/C_{p_o} is 0.5, so that the ratio of the pressure coefficient in the juncture to the two-dimensional value of the pressure coefficient on the wing is 2, as predicted by the linearized theory. Furthermore, the two-dimensional value of C_p/C_{p_o} observed on the wing for this configuration agrees well with the value observed for the case of +8° angle of attack and 135° dihedral angle.

3. Effect of a Gap between Wing and Body

Several runs were made with various gaps between the wing and the body simulator plate. With the angle of attack of the wing at +8 and -8° the gap between the wing and the body was set at 0.10, 0.25, and 0.50 inch. These are the nominal gap settings; actually the gap may vary as much as ± 0.01 but the variation for any one series of runs is ± 0.005. These runs, in conjunction with the runs mentioned earlier with zero gap, then give configurations with four different gap settings.

Care must be exercised in comparing the body pressures for any nonzero gap at a negative angle of attack with the body pressures for the same gap at a positive angle of attack, since the two cases are not directly related due to the effect of the wing profile which is present for nonzero gaps.

a. Pressures Measured on the Body. The pressures recorded on the body simulator plate are again plotted in conical coordinates, i.e., C_p/C_{p_o} versus $\beta r/x$, not because the flow is expected to be conical but for convenience in comparing these data with the data previously discussed for the zero-gap case. The conical coordinate system is attached to the wing so that the x axis lies along the inboard edge of the wing (see Fig. 4). Thus the r in the expression $\beta r/x$ is given by,

$$r = \sqrt{(g)^2 + (y)^2} \quad .$$

where g is the gap dimension (see Fig. 4) and y is the vertical distance in the plane of the body plate from the orifice to the wing plane.

For each gap setting and for each angle of attack the experimental points are shown in Fig. 9. Curves have been faired through these points for values of x = 1.0, 2.0, 3.0, and 4.0 inches at -8° angle of attack and for values of x = 1.0, 2.0, and 3.0 inches at +8° angle of attack.

The faired curves for all gaps are shown in Figs. 10 and 11, in which each value of x is compared with the linearized theory for zero gap. When the wing is at -8° angle of attack the effect of a gap is to cause the pressure on the body plate to rise at smaller values of $\beta r/x$ for larger gaps. Furthermore, the pressure does not rise to as high a value as it does for zero gap as shown below:

x, inches	Percent of Zero-Gap Pressure Values for 0.10-inch Gap	0.25-inch Gap	0.50-inch Gap
1.0	71	58	--
2.0	79	72	71
3.0	88	87	81
4.0	92	83	78

These figures indicate that near the leading edge of the wing the effect of gap is fairly strong but as x increases the effect of gap on the body pressure decreases. This is undoubtedly due to the fact that at the leading edge of the wing the gap is effectively infinite but as one moves farther aft the body plate tends to isolate the upper and lower surface more and more, although never completely.

Figure 11 shows the results for various gap sizes when the angle of attack of the wing is +8°. The shape of the pressure curves on the body alters radically even for the smallest gap. The pressure on the body plate begins to drop much the same as for the zero-gap case. The pressure then levels off at a

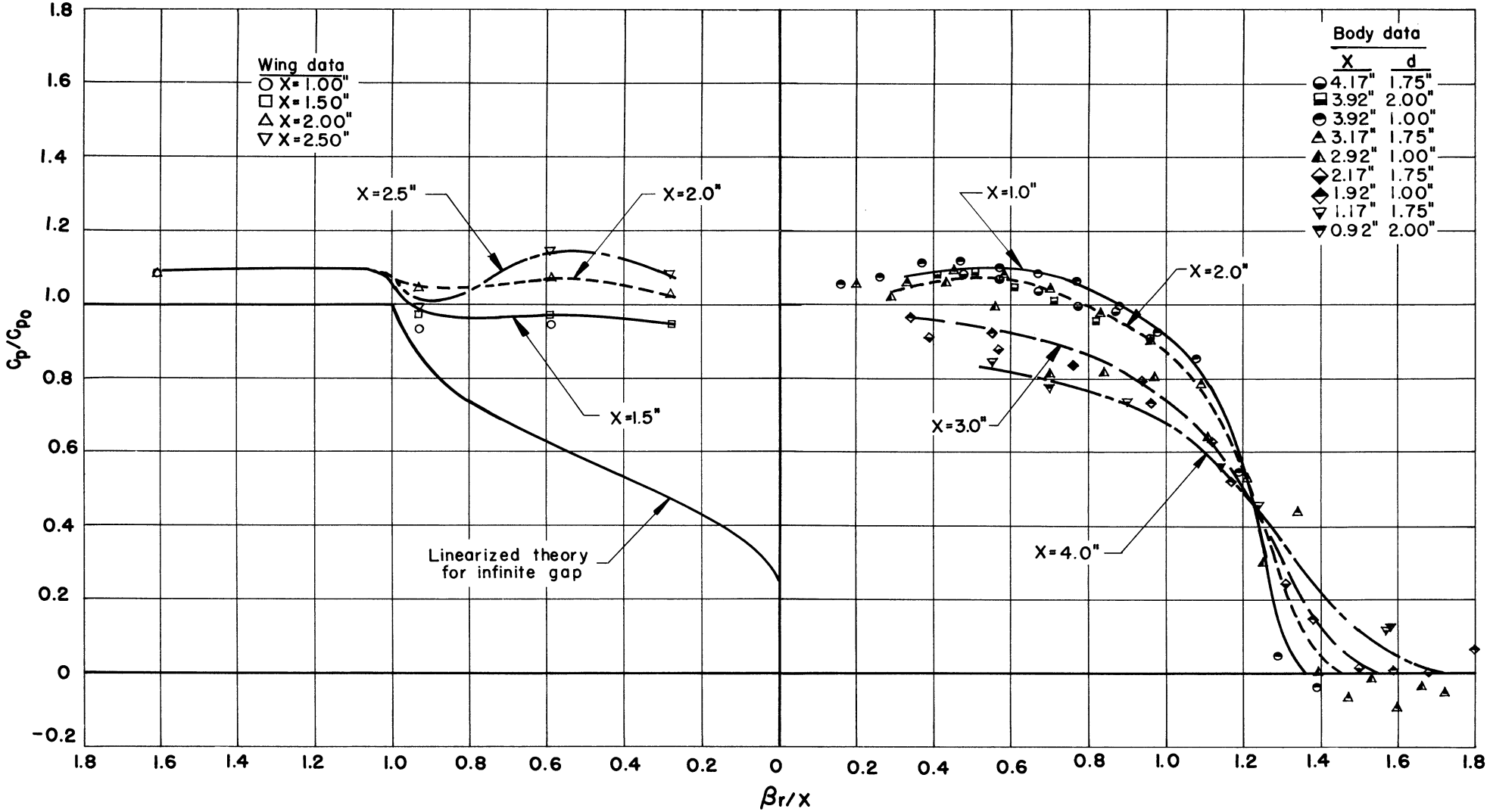

Fig. 9a. Experimental data in conical coordinates: 10" gap, $\phi = 90°$, $\alpha_w = -8°$.

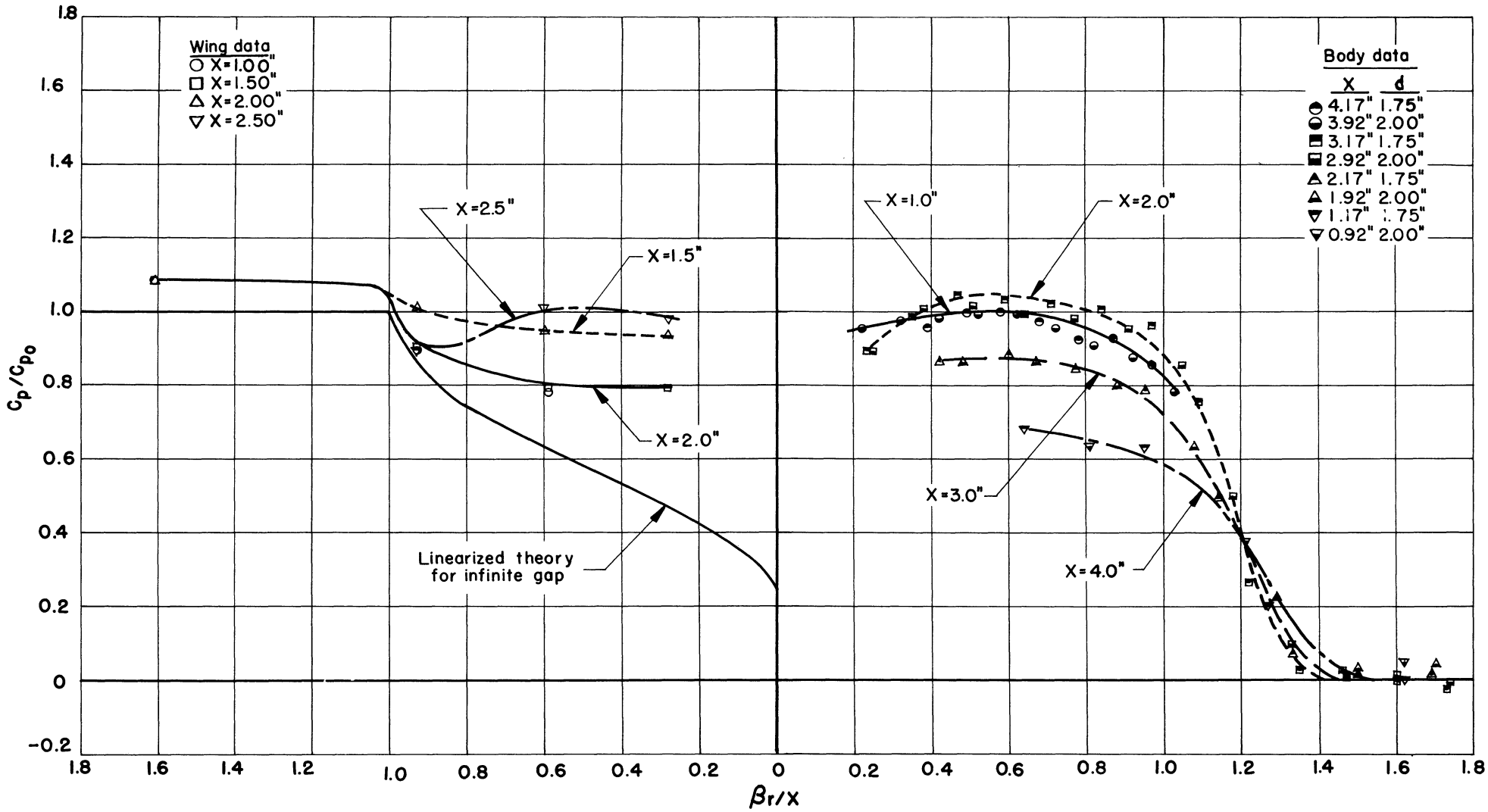

Fig. 9b. Experimental data in conical coordinates: .23" gap, $\phi = 90°$, $\alpha_w = -8°$.

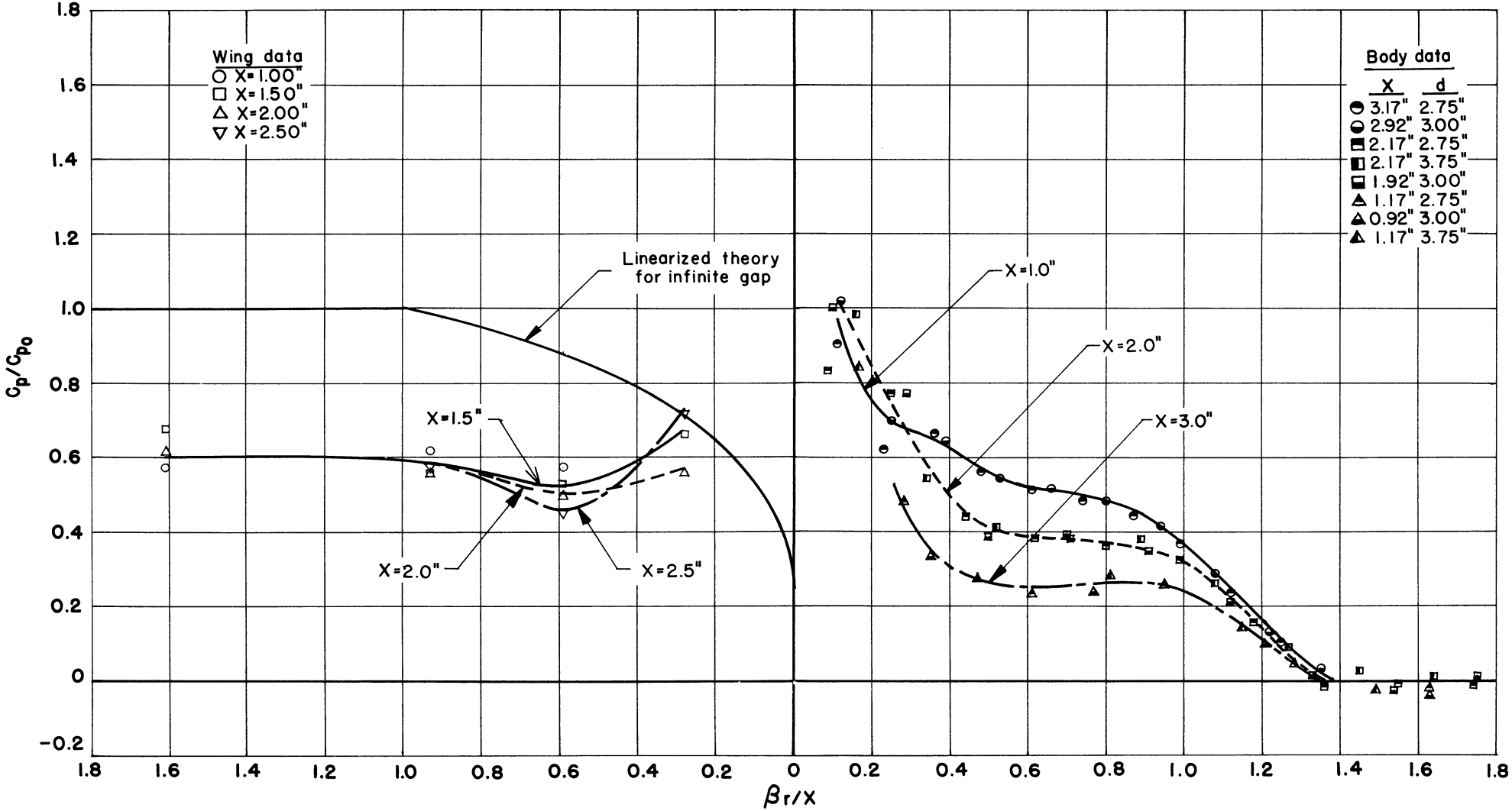

Fig. 9d. Experimental data in conical coordinates: .08"gap, $\phi = 90°$, $\alpha_w = +8°$.

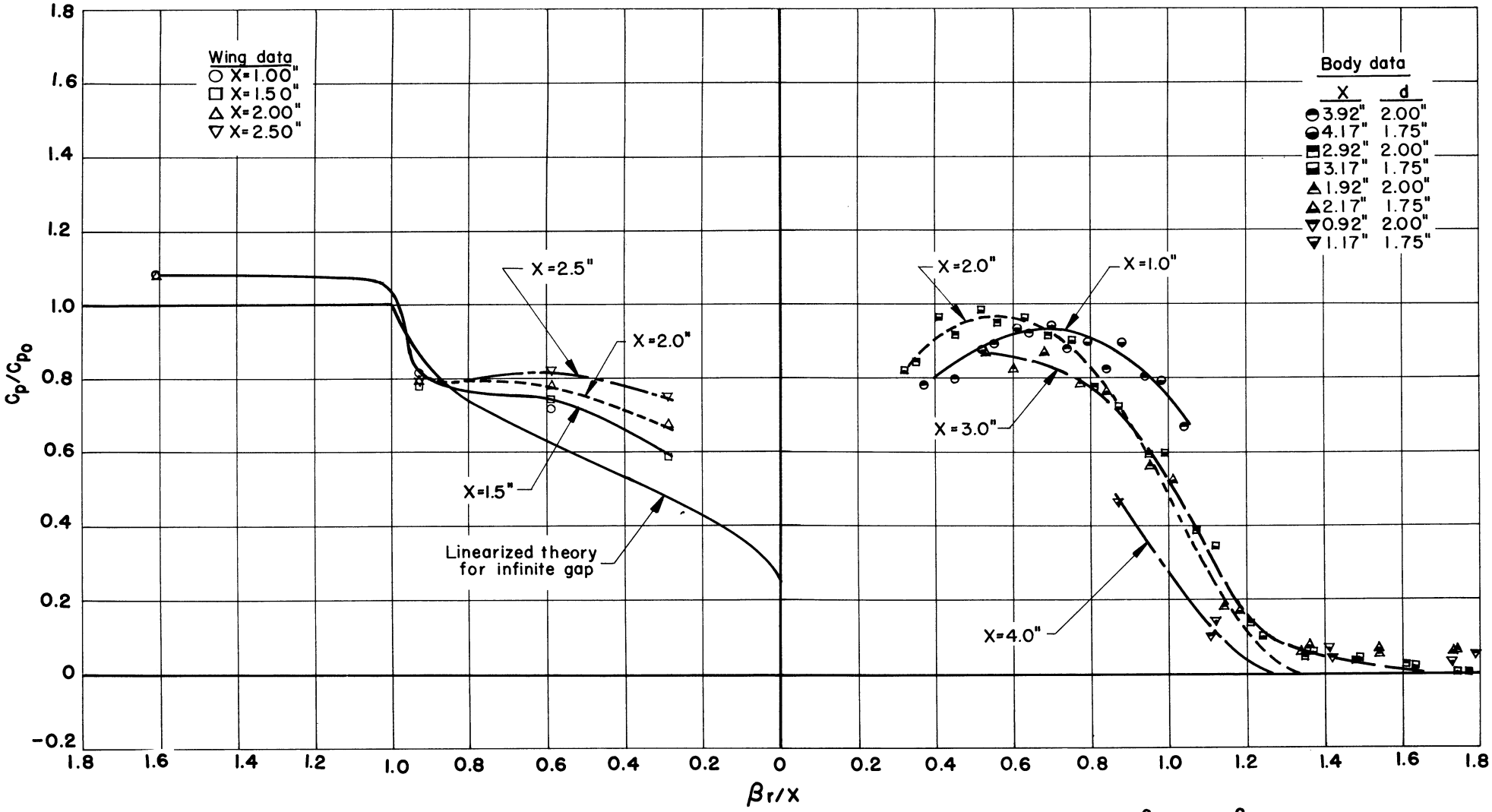

Fig. 9c. Experimental data in conical coordinates: .50" gap, $\phi = 90°$, $\alpha_w = -8°$.

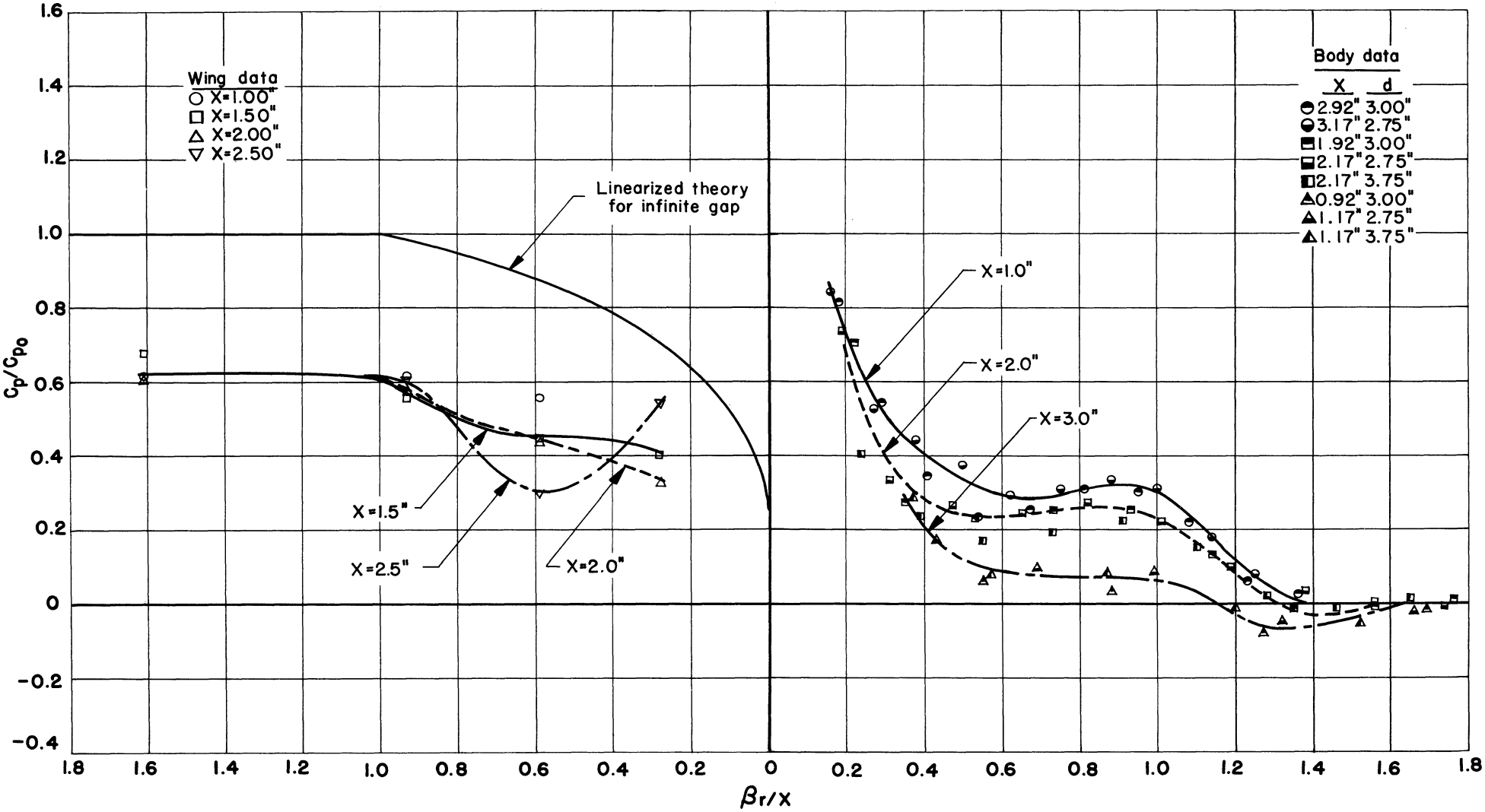

Fig.9e. Experimental data in conical coordinates: .24"gap, $\phi=90°$, $\alpha_w=+8°$.

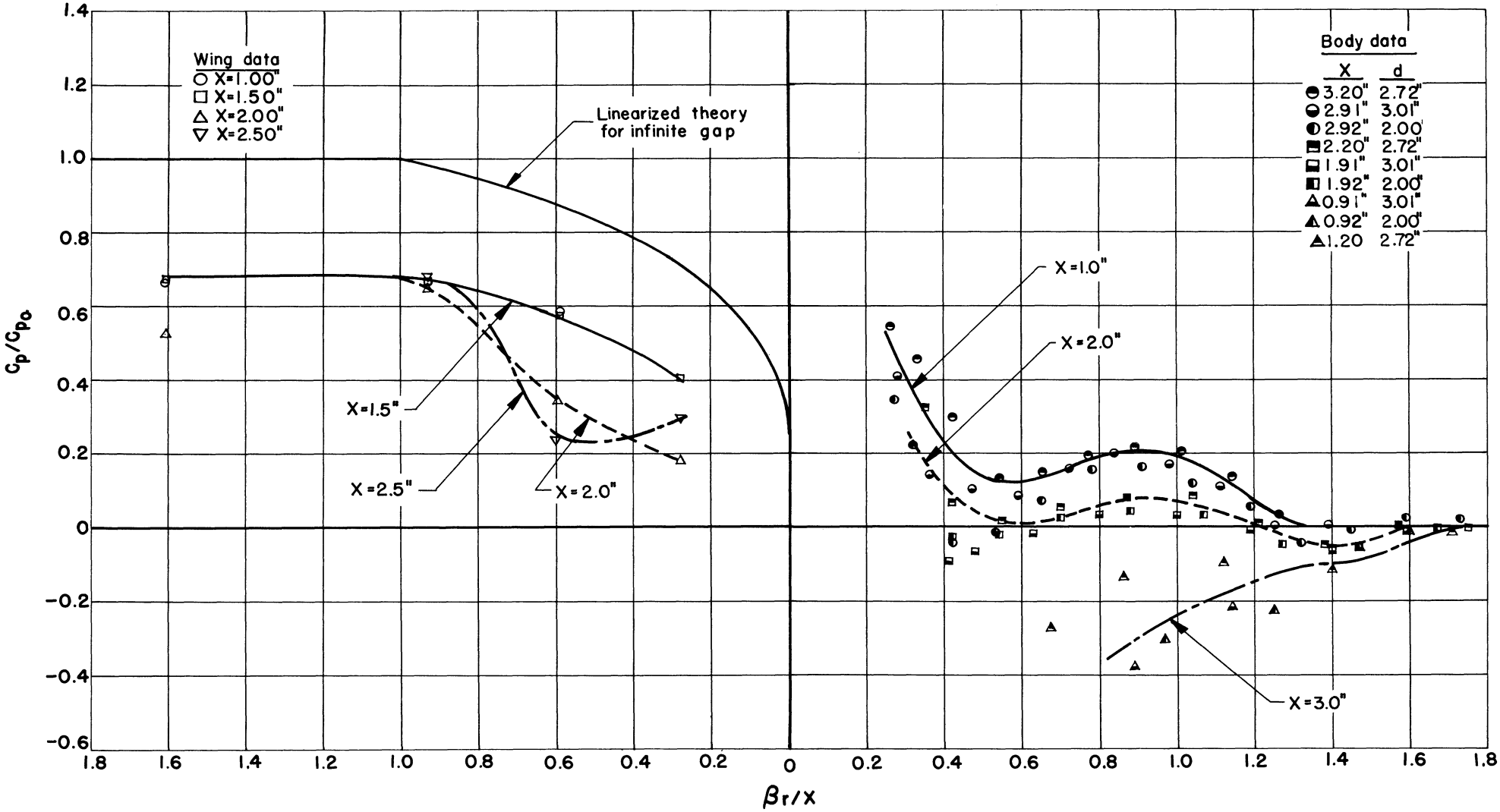

Fig.9f. Experimental data in conical coordinates: .47"gap, $\phi=90°$, $\alpha_w=+8°$.

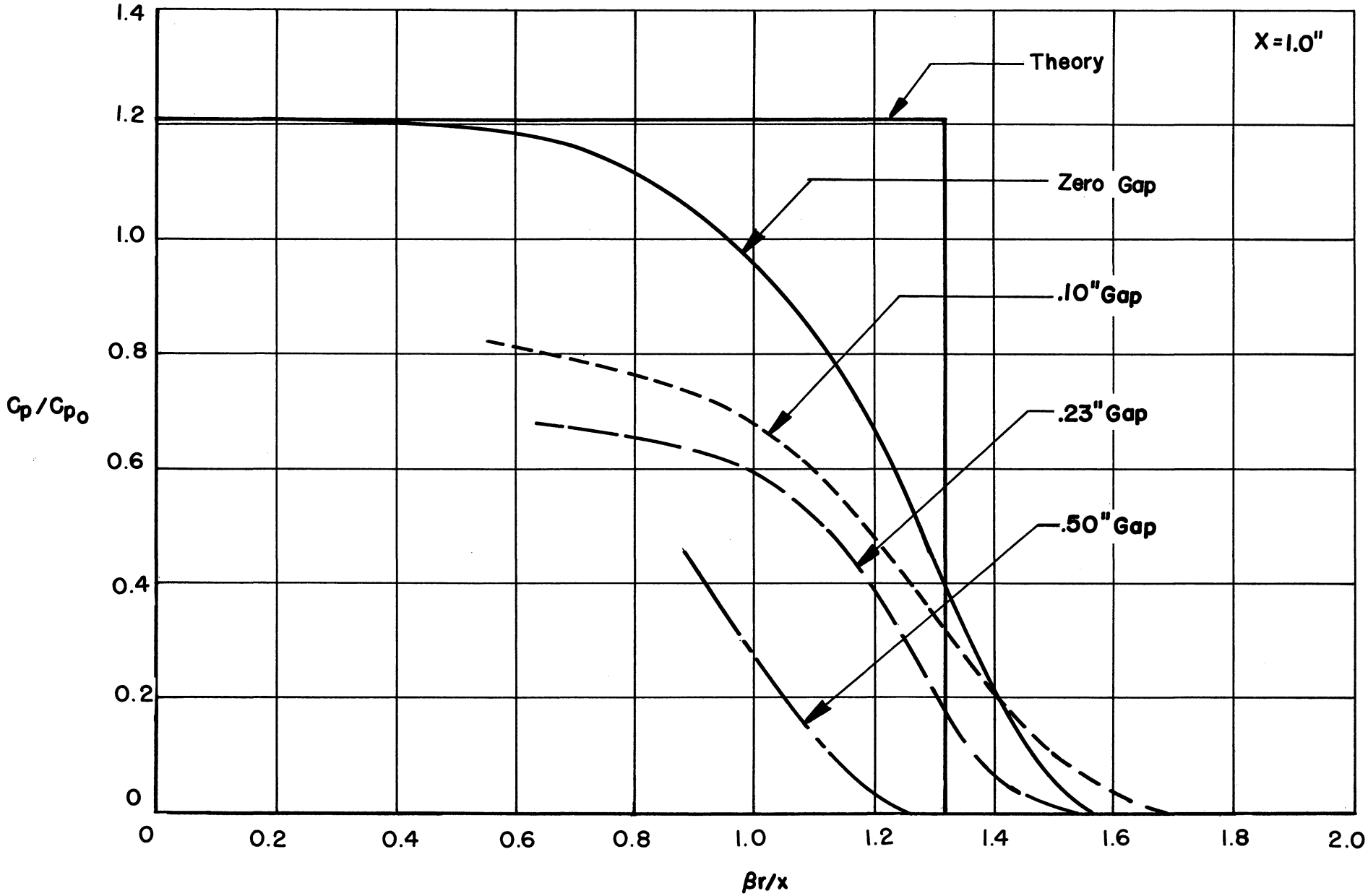

Fig. 10a—Ratio of C_p measured on body plate to linearized C_{p_o} for various gap sizes: $\alpha_w = -8^\circ$, $\phi = 90^\circ$.

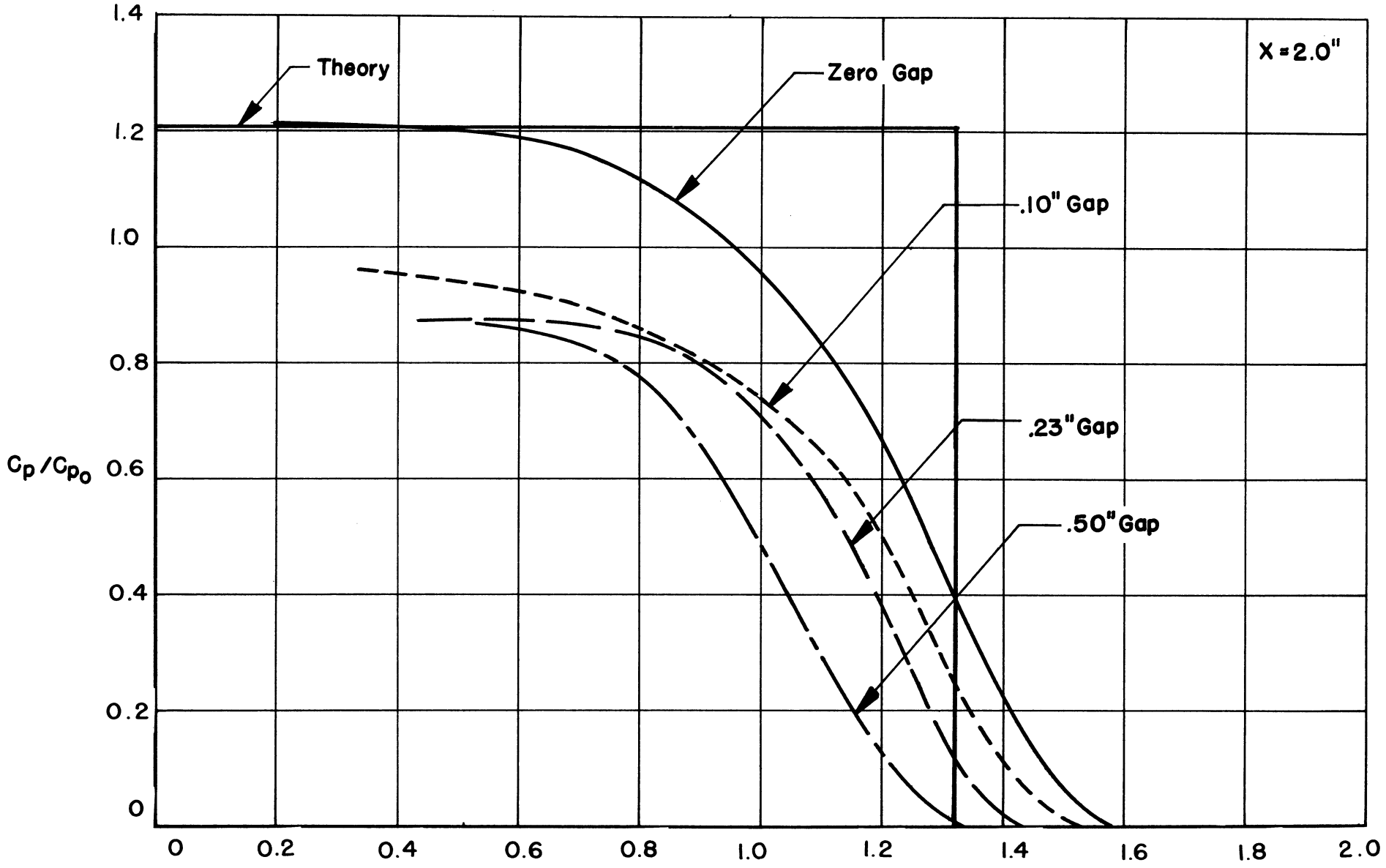
Theory
Zero Gap
.10" Gap
.23" Gap
.50" Gap
X = 2.0"
C_p / C_{p_o}
1.4
1.2
1.0
0.8
0.6
0.4
0.2
0
0
0.2
0.4
0.6
0.8
1.0
1.2
1.4
1.6
1.8
2.0
βr/x

Fig.10 b

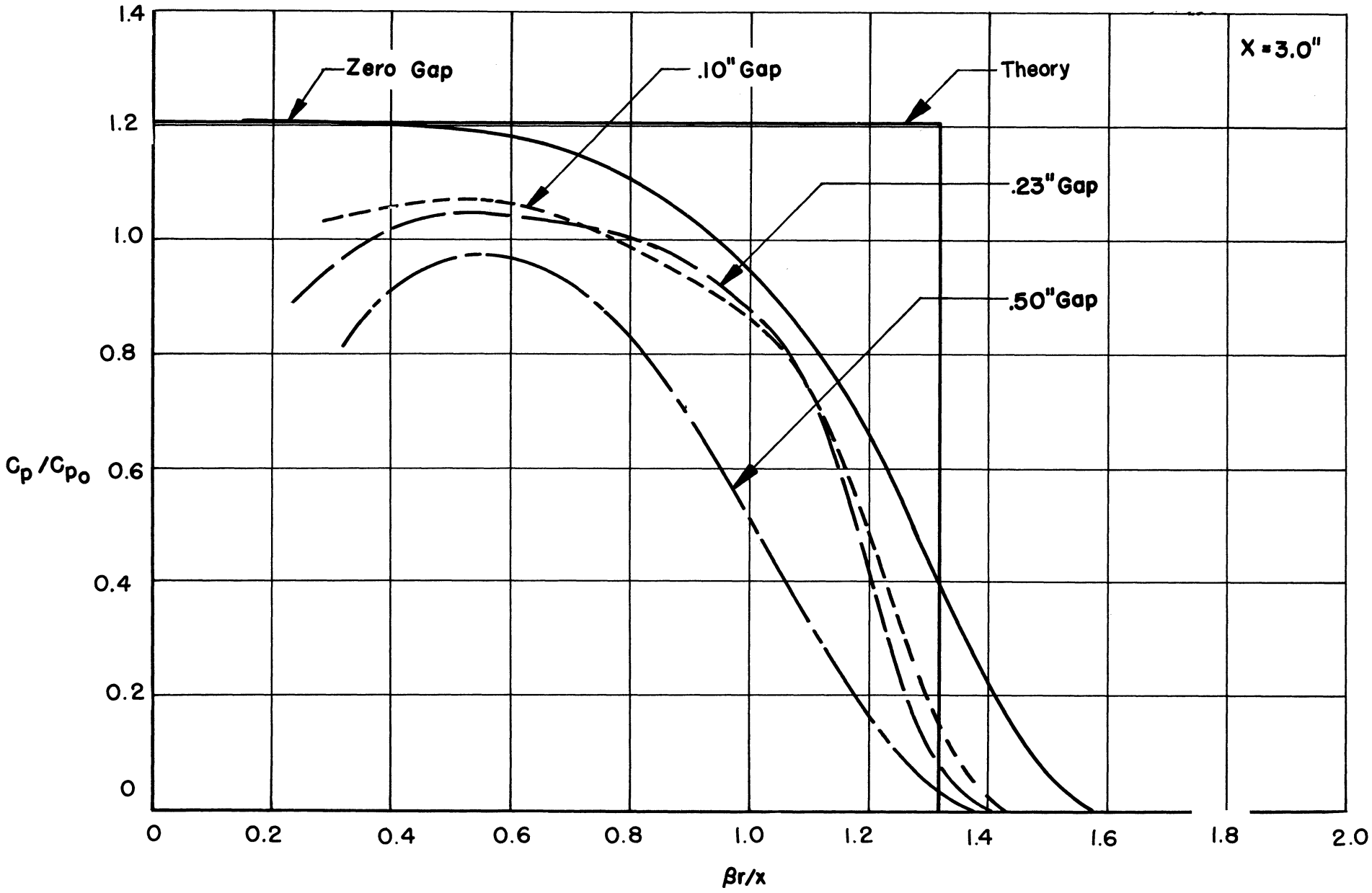
Zero Gap
.10" Gap
Theory
X = 3.0"
.23" Gap
.50" Gap
C_p / C_{p_o}
1.4
1.2
1.0
0.8
0.6
0.4
0.2
0
0
0.2
0.4
0.6
0.8
1.0
1.2
1.4
1.6
1.8
2.0
βr/x

Fig. 10 c

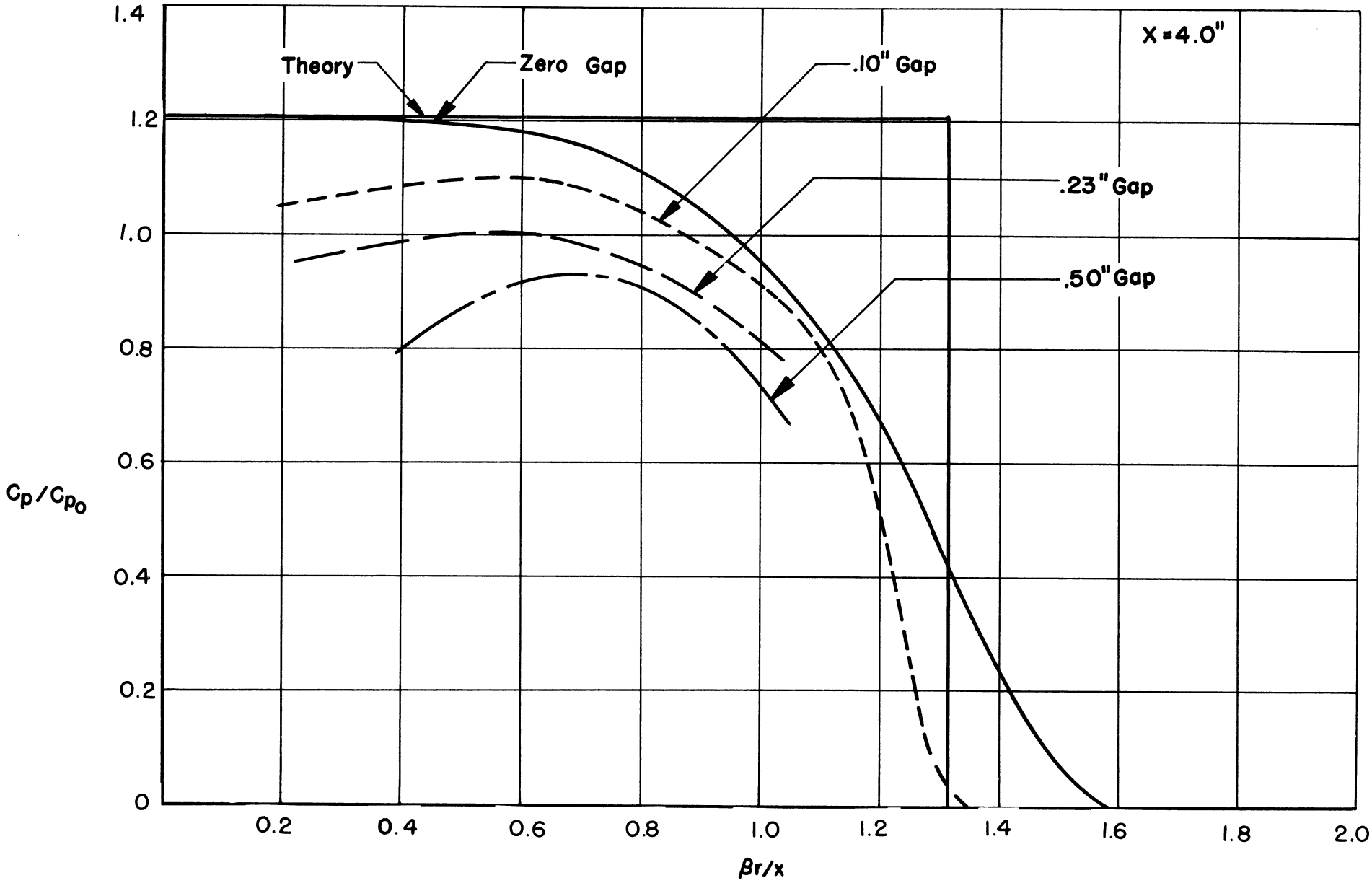
X = 4.0"
Theory
Zero Gap
.10" Gap
.23" Gap
.50" Gap
1.4
1.2
1.0
0.8
0.6
0.4
0.2
0
C_p / C_{p_o}
0.2
0.4
0.6
0.8
1.0
1.2
1.4
1.6
1.8
2.0
$\beta r/x$

Fig. 10 d

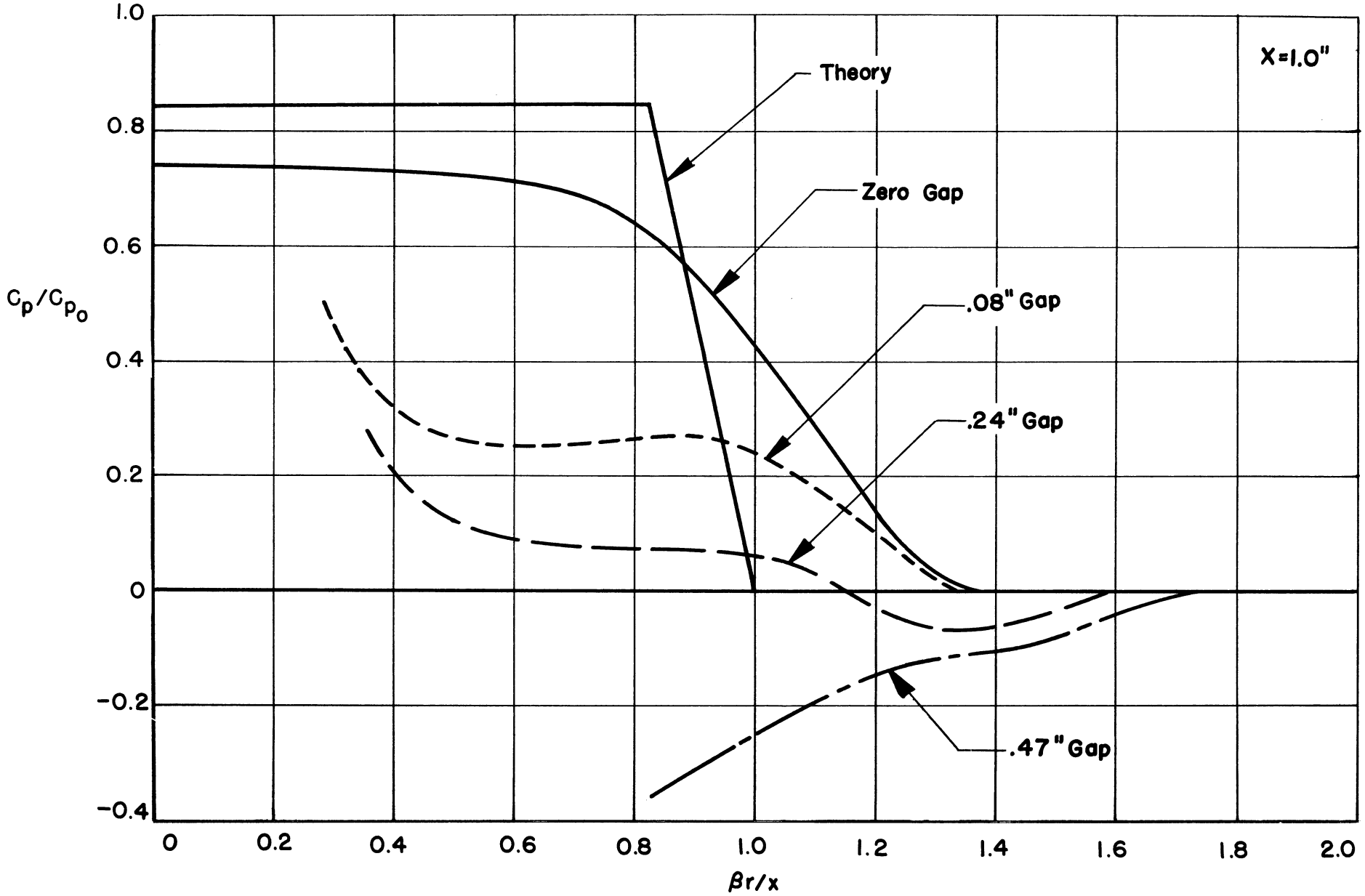

Fig. 11 a — Ratio of C_p measured on body plate to linearized C_{p_o} for various gap sizes: $\alpha_w = +8°$, $\phi = 90°$.

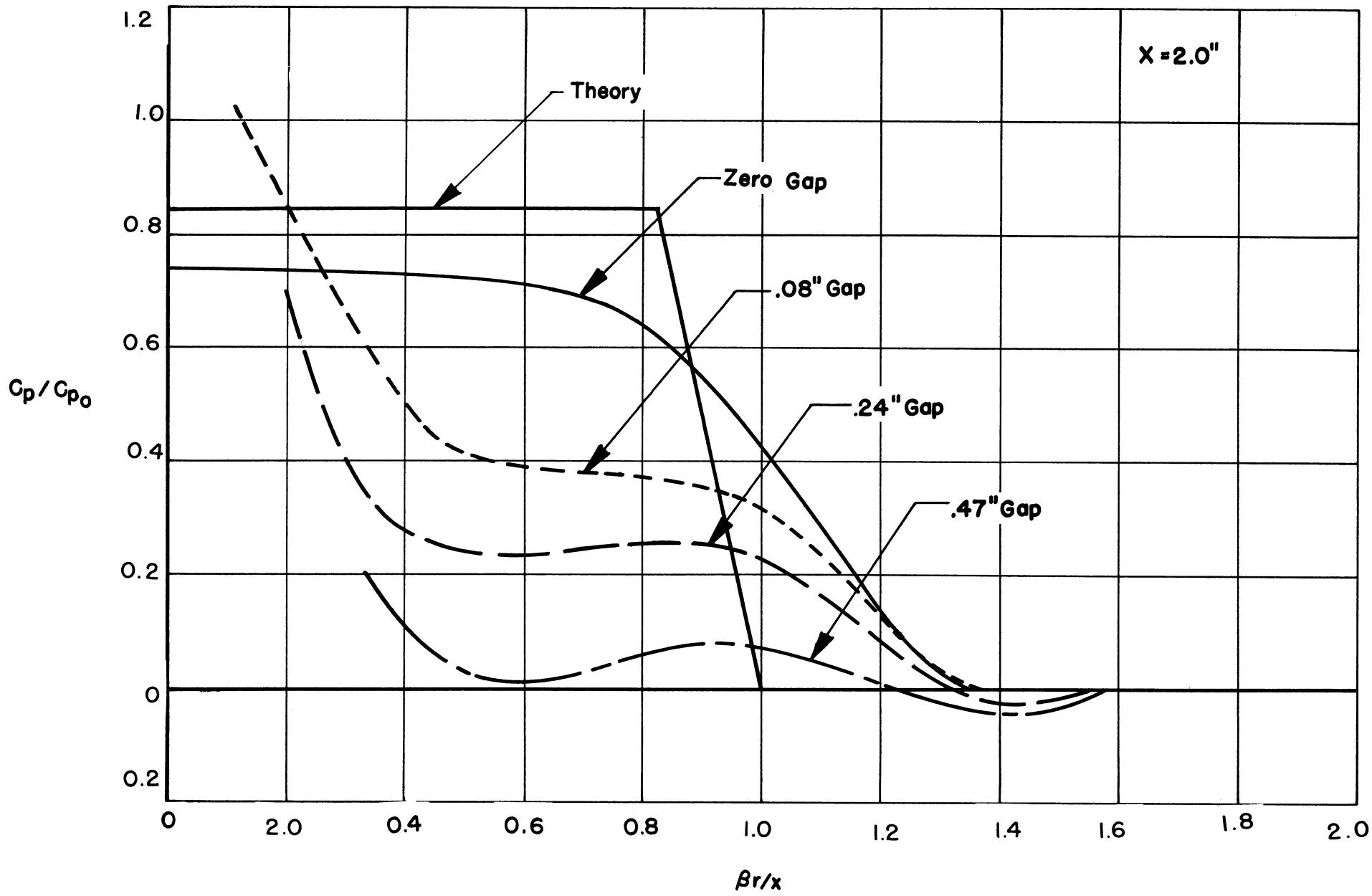
X = 2.0"
Theory
Zero Gap
.08" Gap
.24" Gap
.47" Gap
C_p / C_{p_o}
$\beta r/x$
1.2
1.0
0.8
0.6
0.4
0.2
0
0.2
0
2.0
0.4
0.6
0.8
1.0
1.2
1.4
1.6
1.8
2.0

Fig. 11 b

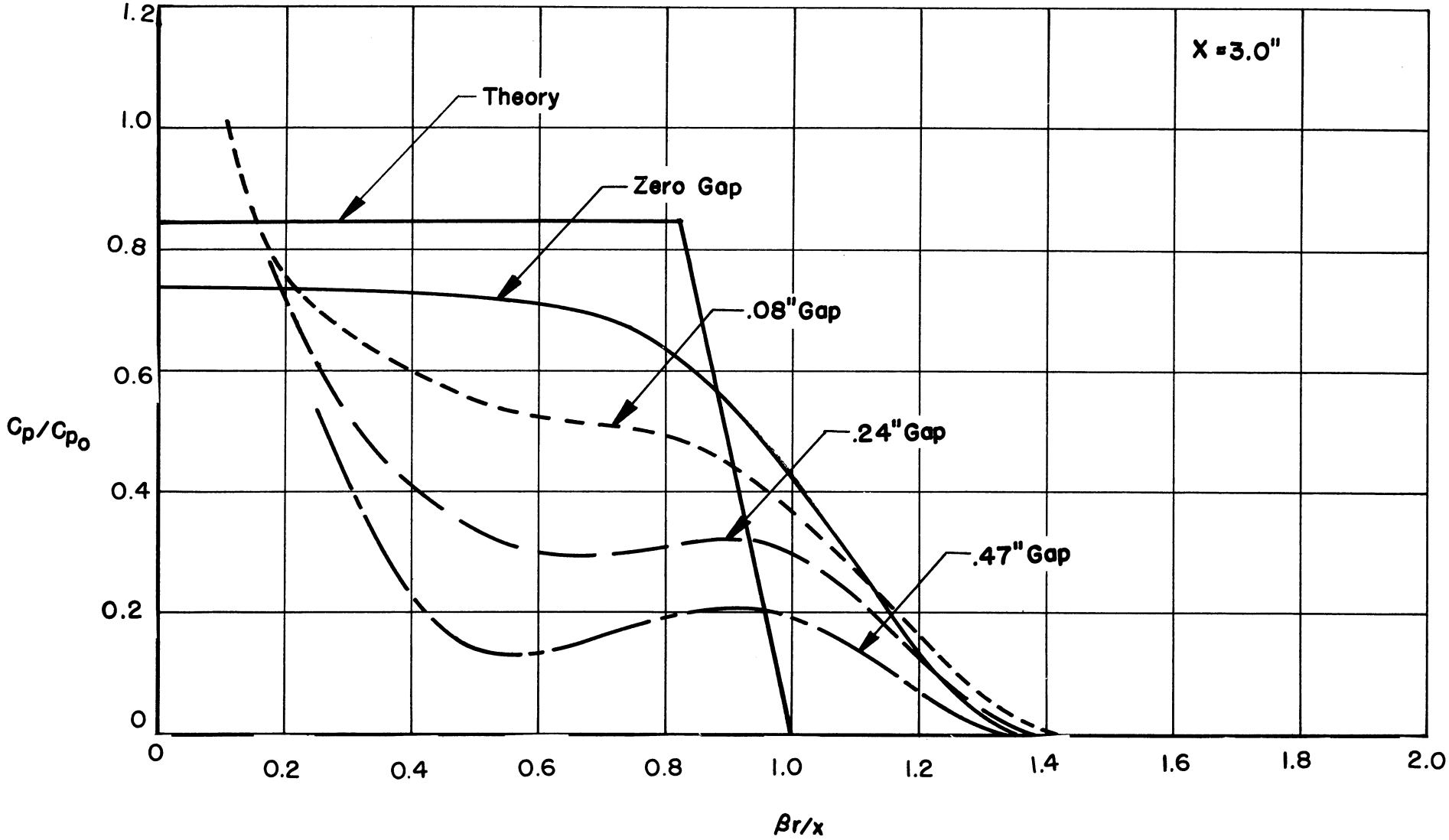
X = 3.0"
Theory
Zero Gap
.08" Gap
.24" Gap
.47" Gap
C_p/C_{p_o}
$\beta r/x$
1.2
1.0
0.8
0.6
0.4
0.2
0
0.2
0.4
0.6
0.8
1.0
1.2
1.4
1.6
1.8
2.0

Fig. 11c

value higher than for the zero-gap case and then at $\beta r/x = 0.5$ the pressure drops to a value well below that for the zero-gap case. It is possible that a wing tip vortex forms in the gap region and then rolls up on the expansion side of the wing. The high velocities induced on the body plate by this vortex then cause the low static pressures which are observed.

In addition to this vortex effect, the plateau pressures which occur just before the extremely low pressures are considerably higher than the two-dimensional value which is measured for zero gap as shown below:

x, inches	Percent of Zero-Gap Pressure Values for 0.10-inch Gap	0.25-inch Gap	0.50-inch Gap
1.0	33	12	--
2.0	51	34	7
3.0	67	41	24

Therefore, while the effect on the body pressure appears to be more severe for positive wing angles of attack than negative wing angles of attack, there is still a tendency for the effect of the gap to become relatively less important for increasing distance downstream of the leading edge of the wing.

b. Pressures Measured on the Wing. The ratios of the pressure coefficients measured on the wing to the two-dimensional pressure coefficient predicted by linear theory are plotted versus $\beta r/x$ in Fig. 9. The value of x, which is the distance from the orifice to the leading edge of the wing, is indicated for each experimental point. As the value of x increases, the pressures measured on the wing vary even for the same value of $\beta r/x$. This variation is probably due to the fact that the top and bottom surfaces of the wing are no longer isolated if there is a gap between the wing and the body.

The data points measured on the wing are not as dense as on the body plate, so that the interpretation of the wing pressures is more difficult. Nevertheless, curves have been faired through the wing pressure data of Fig. 9 and these may be compared with the linearized theoretical curve for infinite gap.

The pressures measured on the wing at -8° angle of attack agree fairly well with the pressures measured on the body plate for the same gap setting. As far as can be determined it appears that the pressure on the wing drops off as the tip of the wing is approached. The pressures measured on the wing ahead of the Mach cone from the wing-tip juncture agree well with the value predicted by theory.

When the wing is at positive angles of attack the two-dimensional value on the wing agrees with that measured on the body plate. The pressures on the wing are quite constant, regardless of the gap size, although there is a slight tendency for an increase in pressure in the region $1.0 \geq \beta r/x \geq 0.6$. There is a tendency for the curves for which x is large to indicate a drop in pressure in the region $0.6 \geq \beta r/x \geq 0.3$. It is quite possible that this is the vortex effect which was mentioned earlier. It is probable that the wing-tip vortex rolls up on the low-pressure side of the wing and counteracts the rise in pressure which would otherwise be expected in this region. This drop in pressure agrees with the pressure trend measured on the body plate where large under-pressures are encountered near the gap.

F. CONCLUSIONS

The experimental pressures measured on the wing and on the body simulator plate agree quite well with the pressures predicted by simple shock-wave and Prandtl-Meyer flow theory. The flow appears to be conical for values of x, the distance aft of the leading edge of the wing, greater than 1. For values of x less than 1 the flow is not conical and the full theoretically predicted pressure jump does not occur. The effect of viscosity is to smooth out to some extent the steep pressure gradients caused by the shock wave at the leading edge of the wing. This gradient is smoothed out more for larger values of x. There is some upstream propagation of the pressure disturbance which originates at the leading edge of the wing, with the amount of upstream propagation increasing for increasing x.

For positive angles of attack of the wing the Prandtl-Meyer flow at the leading edge is preceded by a weak compression shock wave which appears to be a continuation of the shock wave generated on the under side of the wing.

The experimental results obtained with a -8° angle of attack of the wing and a dihedral angle of 135° agree very well with the linear theory of reference 5. The agreement between theory and experiment is also good when the angle of attack of the wing is +8° and the dihedral angle of 45°. However, for the other two cases tested, i.e., (1) angle of attack of the wing +8° and dihedral angle 135° and (2) angle of attack of the wing -8° and dihedral angle of 45°, the agreement between linearized theory and experiment is poor. This poor agreement is probably due to the choking effect on the under side of the wing, with the consequent detachment of the shock wave at the leading edge of the wing. The effects of viscosity are in general the same for dihedral angles of 45° and 135° as they are for a 90° dihedral angle.

The effect of a gap between the wing and the body simulator plate was investigated for three gap sizes in addition to the zero-gap case. For negative angles of attack of the wing the pressures measured on the body are slightly affected and the pressures measured on the wing appear to be quite strongly affected. For positive angles of attack of the wing a wing-tip vortex, which is fairly independent of the gap size, strongly affects the pressures measured on the body plate but apparently compensates for the pressure-relief effect of the gap on the wing, so that the wing pressures appear to be fairly insensitive to the gap size.

REFERENCES

1. Bailey, H. E., and Phinney, R. E., "Final Report, Wing-Body Interference, Part II. Experimental Investigation of Cylindrical Model" University of Michigan, Engineering Research Institute M937-2-F, 1954.

2. Bardsley, O., "The Conditions at a Sharp Leading Edge in Supersonic Flow," Phil. Mag., 42, No. 326 (March, 1951).

3. Liepmann, H. W., and Bryson, A. E., "Transonic Flow Past Wedge Sections," Journal of Aeronautical Sciences, 17, No. 12 (December, 1950).

4. Garby, L. C., and Nelson, W. C., University of Michigan 8 x 13 Inch Intermittent-Flow Supersonic Wind Tunnel, University of Michigan, Memorandum No. 59, Engineering Research Institute, June, 1950.

5. Lagerstrom, P. A., and VanDyke, M D., General Considerations about Planar and Non-planar Lifting Systems, Douglas Report 5M 3432, June, 1949.

6. Snow, R. M., "Aerodynamics of Thin Quadrilateral Wings at Supersonic Speeds", Quarterly of Applied Mathematics, 5, No. 4 (January, 1948).